2014

Investigating Mechanical Properties of Metallic Nanowires using Molecular Dynamics

Alex Khammang
Virginia Commonwealth University

Investigating Mechanical Properties of Metallic Nanowires using Molecular Dynamics

A thesis submitted in partial fulfillment of the requirements for the degree of Master of Science at Virginia Commonwealth University.

By

Alex Khammang

Bachelors of Science, Physics,
Virginia Commonwealth University 2012

Director: Dr. Denis Demchenko,
Assistant Professor, Department of Physics

Virginia Commonwealth University
Richmond, Virginia

May, 2014

Acknowledgments

I wish to thank several people. I would like to thank all of my peers and professors for all of their moral support and technical assistance. I want to especially thank Brandon Child and Christopher Angevine for suffering through the thesis writing and presenting process with me. I would like to thank Anthony Pedicini and Ibrahima Castillo for their endless trouble shooting and technical support. I would like to thank Dr. Marilyn Bishop and Dr. Thomas McMullen for their infinite wisdom during my entire academic career at VCU. I would like to thank my family for their support in education, especially my sister for not being bothered by my all-nighters. I would like to thank Dr. Dexian Ye for the inspiration of the research project. Last but not least I would like to thank Dr. Denis Demchenko for the past three and a half years of research experience, for not firing me when he probably should of, and for his extensive assistance while researching.

Table of Contents

Abstract

INVESTIGATING MECHANICAL PROPERTIES OF METALLIC NANOWIRES USING MOLECULAR DYNAMICS

A thesis submitted in partial fulfillment of the requirements for the degree of Master of Science at Virginia Commonwealth University

By

Alex Khammang, Virginia Commonwealth University, 2014

Major Director: Dr. Denis Demchenko, Assistant Professor, Department of Physics

Metallic nanowires have useful applications in scanning tunneling microscopes and atomic force microscopes due to their unique sensitivity to force and electricity. These unique properties arise because of the large surface area to volume ratio. One of these properties is that introducing twinning planes the mechanical properties of metallic nanowires can be altered. The effects of twinning planes on metallic nanowires were studied using molecular dynamics simulations. Silver, copper, and nickel nanowires with and without twinning planes were simulated with engineering strain until the first yielding stress was obtained. The radial simulations showed that as the radius of twinned nanowires increased, the strength gained by introducing the twinning planes increased. The temperature simulations showed that nanowires with twinning planes were stronger than their un-twinned counterparts as temperature increased. The purpose of this investigation was to better understand the effect twinning planes had on metallic nanowires, so that future technological advances would benefit from the results.

Chapter 1: Introduction

1.1 Literature Review

Metallic nanowires have applications in nano-electromechanical systems, because of their unique sensitivity to physical stimuli, for example being capable of operating under high frequencies. They also have useful applications in scanning tunneling microscope (STM) and atomic force microscope (AFM) for nanoscale tip-sample interactions.[1] These unique properties arise from the large surface area to volume ratios, that is inherent to nano-scale materials. Along with the large surface area to volume ratio, the introduction of twinning planes has shown to affect the mechanical properties of metallic nanowires.[2] Experiments and simulations both show that by introducing twinning in metallic nanowires planes, ductility, elastic moduli, and yielding stress change.

Experiments show that metallic nanowires can be stronger than their bulk counterparts. Marcel et al.[3] have shown silver nanowires to have a higher yield stress than the bulk. The yield strengths of gold whiskers have been reported over ten times stronger than the bulk.[4] The yielding of the nanowires can be described through molecular simulations as a series of yielding events until failure. The findings of Marcel et al.[3] also suggest that as nanowire diameters decrease, the yield strength increases for diameters less than 10nm. For diameters greater than 10nm the yield strength approaches the bulk values. Nath and Kim's experiment on gold nanowires shows similar radial dependences on the yielding strength.[2] This phenomenon can be attributed to their large surface to volume ratio.

The surface atoms have lower coordination numbers than the core atoms. Surface atoms produce a higher stress, because of the inherently large surface area to volume ratio. Since the nanowires are so small the number of core atoms cannot oppose the amount to surface stress like in the bulk, thus compressing the wires. A number of studies have shown this effect[5,6,7] and suggest that this larger surface area to volume ratio influence the mechanical properties of ductility, elasticity, and yielding. The larger the surface area to volume ratio, the more surface strain should act on the body, thus producing higher yield stress.

Growth experiments show that twinning planes are a naturally occurring defect in metallic nanowires. Since twinning planes occur naturally, the study of their effects on metallic nanowires is crucial in understanding the mechanical properties of these systems. The nucleation process begins at the surface, to initiate the dislocation nucleation, and then the dislocation will propagate through the nanowire until it reaches a free surface.[8,9] Studies have shown that twin boundaries interrupt the glide of dislocations[1], thus delaying the propagation of partial dislocations. In principle, twin boundaries delay the glide of partial dislocations until enough stress is applied so that the dislocation breaks through the boundary and reach the free surface.

Using molecular dynamics, Deng and Sansoz[10] discovered three different mechanisms for the propagation of partial dislocations. Deng and Sansoz[11] also suggest that certain embedded atom potentials will show strain-hardening after the initial yield point, while other potentials show only strain-softening. When running molecular dynamic simulation, the choice of potentials is important. The choice of embedded atom potential can produce completely different results for the same material. Depending on the potential, different yielding mechanisms may be more dominant.

For mechanism I, the glide of the leading partial dislocation is emitted from the surface and is stopped immediately by the coherent twin boundary. Due to the dislocation blockage, significant strain-hardening occurs in nanowires with this mechanism. The maximum flow stress is reached when secondary partial dislocations are able to emit from different defects on the free surface. This phenomenon appears to be consistent with GRS potentials.[10] The energies predicted by the potentials suggest that the nucleation energy is lower than the energy required for yielding.

For mechanism II, the leading partial dislocations emitted from the surface are directly transmitted though the coherent twin boundaries. The yield stress and the max flow stress are thus the same. This implies that the yielding energy and nucleation energy the same or nearly identical. In mechanism III, the first leading partial dislocation emitted at the yield point is accompanied by the nucleation and propagation of a twinning partial dislocation on a plane parallel to the slip plane. Both types of dislocations appear to transmit and become part of the twining plane. This last mechanism was noticed for aluminum potential.[10] Researchers should be careful when measuring the mechanical properties of metallic nanowires.

Figure 1.1.1 depicts the movement of a slip plane that is blocked by a twinning plane. The edge of the slip plane is marked in blue and the twinning plane is marked in red. After the nucleation from the surface, the partial dislocation propagates through the nanowire until it encounters an obstacle, in this case a twining plane. Depending on the material, mechanism I or mechanism II are likely occur for Foiles' potentials.

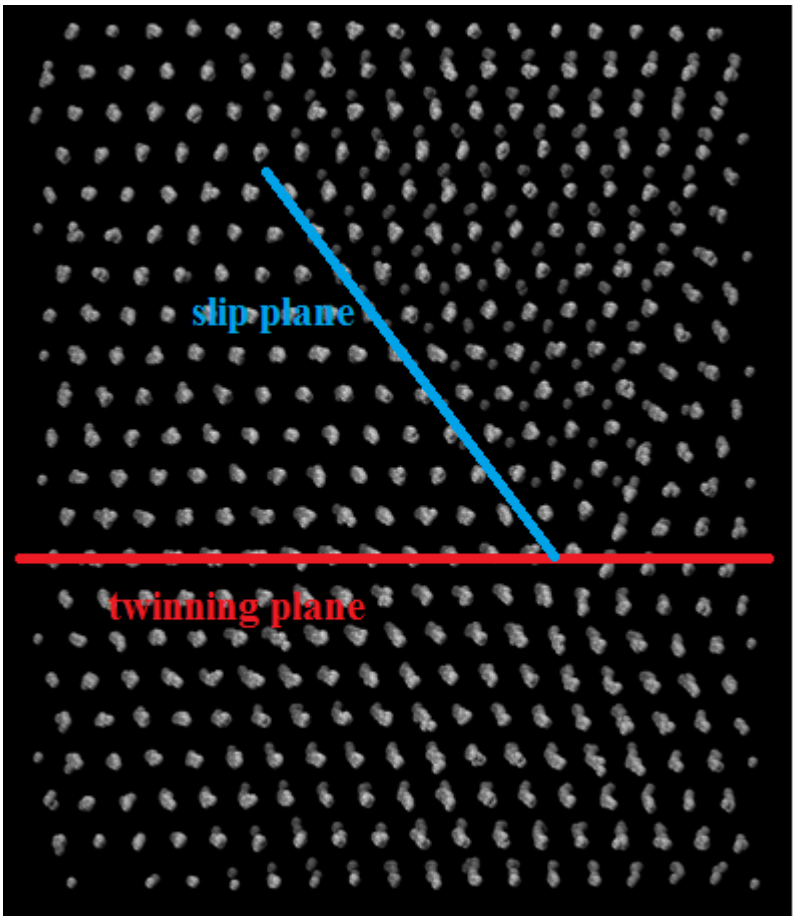

Figure 1.1.1: Depiction of slip plane impeded by twin boundary.

In experiment, scanning electron microscope (SEM), transmission electron microscope (TEM), and atomic force microscopes (AFM) are common tools for performing mechanical tests on nanowires. Since the act of applying tensile strain at the nanoscale is difficult to perform in lab, indirect force displacement tests on the midpoint of the nanowires are performed on the nanowires to measure the mechanical properties. Wu et al.[4] claim that experimentally, the measured failure could be attributed to the wire itself or contact between AFM tips or substrates. This could lead to overestimation or underestimation of the yielding stress.

For molecular dynamics, programing tensile straining is not an issue. This makes molecular dynamics simulations to be a very powerful tool for investigating mechanism and

mechanical properties of nanowires. There are major considerations that need to be address prior to molecular simulation work, like the type of potentials or the strain rate that the tensile test is performed with. Potentials used in molecular dynamics, such as EAM, take into consideration an approximated many-body interaction of atoms, which are absent in pair potential schemes.[12] According to Deng and Sansoz[10], depending on the type of potential used, the results may vary significantly.

Another important control is setting an appropriate strain. Wu et al.[12] have shown that when strain rates are low, less than $10\times10^{8}s^{-1}$, then the yield stress do not change drastically. The low strain rates show multiple slips with increasing tensile strain until necking and failure. When strain rates are high, larger than $10\times10^{8}s^{-1}$, then amorphization and super-plasticity occur, which does not lead to meaningful elastic moduli, yielding stress, or mechanical failure. Wang et al.[13] showed similar behavior for nickel nanowires and claimed that a higher strain rate produces a non-linear elastic regime. If the strain rate is very high during the stretching process, the nickel atoms will not have enough time to respond to the forced movement to reach a new equilibrium positions, thus leading to early fracture.

In general, by decreasing the twin spacing, the yielding stress increases. A literature reports suggest a power law increase of yield strength with decreasing twin spacing.[14] On the other hand, when the twin boundary spacing is equal to or greater than the nanowire diameter, twin boundaries have shown no influence on the mechanical properties of gold nanowires.[8] Reports suggest that when the number of twinning planes is greater than two, with decreasing the twin interspacing to less than or equal to the nanowire diameter, the material strength increases.[8,9] With decreasing the twin spacing, the higher the probability of partial dislocations have of encountering a twinning plane before escaping at the surface. This agrees with the

results from Cao et al.[15] have reported that twin spacing have an inverse relationship with the yielding stress. As the spacing of twinning planes decreases, the yielding stress increases. The results also suggest that the smaller the spacing, the less ductile the nanowire becomes.

The source of dislocations affects the yield strength of the nanowires, Wu et al.[14] have simulated copper nanowires with and without twinning planes and found that they nucleate at about the same stress. This suggests that dislocations are emitted from the surface. In another set of simulations, artificial defects were introduced to surface defects on the wires. The findings suggest that the yielding stress was lower for both wires as dislocations required less energy to nucleate at the surface. This finding also suggests that twinning plane densities have little effect on strengthening. Only about a 1% difference in yielding between twin and un-twinned wires was observed.

There are also some cases when even increasing the number of twinning planes won't affect the strength. Zhang and Huang[1] showed that the morphology of the nanowire affects the strength of the nanowire. Using molecular dynamics to investigated copper nanowires with circular and square cross-sections showed that nanowires with square cross-sections have lower nucleation dislocation energies than the yielding stress. This leads to strain hardening with twinning planes. The sharp edges are believed to emit dislocations at lower energies. The circular nanowires have dislocation nucleation energy very similar to yielding energy which does not lead to strain hardening with twinning planes. These results could explain the results of Wu et al.[14], since the wires were circular in shape, the results would not show any major strengthening with different twinning plane densities.

The results of Zhang and Huang[1] also showed that for square cross-section the yielding stress increases as twin spacing decreases while for circular cross-sections the yielding stress is

more constant as twin spacing decreases. For the square cross-sections, strain hardening occurs because the energy required for the dislocation to penetrate the twin boundary is greater than the energy required to nucleate. Strain softening occurs because the dislocation nucleation energy is nearly identical to the yielding energy, thus the twinning boundary is unable to inhibit the propagation of the dislocation.

Another way of measuring the strength of the nanowire is to compare the Young's moduli of metallic wires. By considering the previous results, where the yielding stress is inversely proportional to the nanowire diameter, the Young's modulus could also be inversely proportional. Jing et al.[5] have shown experimentally that the Young's modulus is inversely proportional to the nanowire diameter for nanowires in the range of 20 to 140 nm, which means that the Young's modulus increase as the nanowire diameter decreases. Zhu et al.[7] also report that the Young's modulus increases as the diameter of their nanowires decreased. It may follow that the Young's moduli of all metallic nanowires follow the same relationship.

Since the nanowires are extremely small, molecular dynamics simulations play an important role in understanding the mechanisms involved with the yielding of metallic nanowires. Through molecular dynamics, the stress-strain curves of metallic nanowires reveal an initial yield followed by quasi-elastic events.[16] The results of Pastor-abia et al.[16] show that with averaging these quasi-elastic events average to a constant value well below the initial yield point. This then further implies that no strain hardening actually occurs. This contradicts other molecular simulations; maybe averaging does not offer an exact, realistic measurement, but rather a more definitive answer to whether strain hardening occurs in nanowires or not.

The study of metallic nanowires has shifted towards studying the mechanical properties of composite metallic nanowires. A study by Alavi[17] found that the stress versus strain curves

can be described by Hook's law. With that, the Young's modulus decreases with increasing strain rates and that the modulus increases with temperature. Ma et al.[18] investigated the properties of copper nickel nanowires and found that the elastic modulus and yield strength decreased with increasing copper nickel layer thickness. Due to the lattice misfit, copper layers experience additional tensile stress while nickel layers experience compressive stress in the wire length direction because of Poisson's effect. In other words, since the copper atoms are spaced smaller than their bulk spacing in the x and y directions, they experience a tensile stress in the z direction of the wire.

Since the nickel atoms are spaced relatively wider than the bulk spacing they experience compressive stress in the z direction. Ma et al.[18] report that copper has a much lower yield stress than nickel. Interestingly they found that by forming a composite wire, the yield stress of the wire is actually stronger than copper, but weaker than nickel. They suggest that the destructive lattice distortions take place in the copper layers first and propagate into the nickel layers after enough stress is applied. The nickel layer acts similarly to a twin boundary, impeding the flow of dislocation to the surface.

An important study of metallic nanowires is the effect of temperature on them. A major issue with temperature has been reported with annealing nanowires on substrates and performing mechanical tests. The annealed nanowires showed lowered yield stress than their non-annealed counter parts, which adds to the difficulties in experiments. In molecular dynamics, reports from Sun et al.[19] claim that metallic nanowires exhibit higher yield stress at colder temperatures. The lower the temperature, the lower the energy of the system, which means the more stress would be required to nucleate a dislocation. At higher temperatures the thermal motion of the atoms is more intense, which generates greater amplitude of oscillations around the equilibrium positions.

This leads to lower attractive forces between atoms and they thus the bonds are more easily broken.[13] To ensure reasonably accurate results with molecular dynamics strain rates much be chosen carefully. When comparing temperatures, if the strain rate is too high then at lower temperatures the wire will rupture faster.

The goal of this work is to use molecular dynamics to better understand the mechanical properties of copper, nickel, and silver nanowires with radii ranging from 20 to 50 Angstroms and to investigate the effects of temperature on these metallic nanowires. The radial simulations agree that by introducing twinned boundaries into copper, nickel, or silver nanowires, strengthening effects occur. The temperature trial suggests that metallic nanowires with twinning planes perform better than the un-twinned counterparts at higher temperatures. The majority of experiments have been conducted on nanowires much larger than those simulated here. Nevertheless, the results of these simulations should to help guide future interests in constructing nano-electromechanical devices with nanowires at this scale.

Chapter 2: Methods

2.1 Theory of Molecular Dynamics

The core of all molecular simulation methods is a potential energy function *U(R)*. It determines the potential energy of a system of N atoms, as a function of all atoms and the correlated positions. The bonded potential function U_{bonded} usually takes form[20]

$$U_{bonded} = \sum_{bonds} \frac{K_b}{2}(b - b_0)^2 + \sum_{bond\ angles} \frac{K_\emptyset}{2}(\emptyset - \emptyset_0)^2 + \sum_{dihedral\ angles} \frac{K_\tau}{2}(1 - \cos(3\tau - \tau_0)). \quad (2.1.1)$$

Here, b, ϕ, and τ are the values of bond distance, bond angle, and dihedral angle respectively and that $b_0, \phi_0, \text{and } \tau_0$ are equilibrium constants. Also note that $K_b, K_\emptyset, \text{and } K_\tau$ are the corresponding force constants. The terms of equation (2.1.1) include interactions involving two atoms (the bonds), three atoms (the bond angles), and four atoms (the dihedral angles)[20], which interact with each other to provide the bonded potential energy potential.

The atoms of a system which are further apart in terms of bonding interactions and atoms belonging to different molecules are normally treated as non-bonded interactions. These are usually taken to be pairwise interactions. The non-bonded potential function usually takes the form[20]

$$U_{non-bonded} = \sum_{non-bonded\ pairs} 4\varepsilon_{ij}\left[\left(\frac{\sigma_{ij}}{r_{ij}}\right)^{12} - \left(\frac{\sigma_{ij}}{r_{ij}}\right)^{6}\right] + \frac{1}{4\pi\varepsilon_0}\frac{q_i q_j}{r_{ij}}. \quad (2.1.2)$$

The r^{-12} term in equation (2.1.2) approximates the repulsion between the filled electron shells, the r^{-6} term accounts for the attraction between atoms (London forces), and the r^{-1} term is the

Columbic attraction or repulsion of the two atomic partial charges q_i and q_j. The r terms, r^{-12} and r^{-6}, together are better known as the Lennard-Jones Potential. Lastly the terms ε_{ij} and σ_{ij} are referred as the zero point and well depth.[20]

The gradient of the potential energy function with respect to the position of every atom, *i*, is given as follows[20]

$$\nabla_i U(r) = \frac{\partial U(r)}{\partial r_i}. \tag{2.1.3}$$

For different molecular simulation methods, the potential energy and/or its gradient will be used differently. If only the gradient of the potential is used, then the molecular system will be pushed towards nearest local minimum. This is normally called energy minimization, geometry optimization, or molecular mechanics. If the atoms influenced by their masses as well as the potential energy gradient, then the motion will be partially determined by inertia.[21] This means that the atoms will follow Newton's second law

$$F_i(t) = m_i \frac{\partial^2 r_i}{\partial t^2} = -\nabla_i U(r). \tag{2.1.4}$$

Using Newton's second law, the equation of motion is the basis of *molecular dynamics.* Molecular dynamics (MD) simulations compute the motion of molecules in models of solids, liquids, and gases. The basic idea behind MD is to measure, manipulated, and control observables. To measure observables, the MD simulations assign numerical values to the system's individual states, like the position of atoms. Then, the configurations of the system are generated by integrating Newton's laws of motion. This results in a trajectory that specifies how the positions and velocities of the particles in the system vary with time.[22] Newton's laws of motion can be stated as follows: a body continues to move in a straight line at constant velocity

unless a force acts upon it, a force equals the rate of change of momentum, and to every action there is an equal and opposite reaction.[22] These positions of atoms are calculated by numerically integrating Newton's second law equation (2.1.4).

The positions reveal the dynamics of individual atoms, by printing out the individual atoms and then, by stringing the positions together one can recreate a system's development with time. Integrating Newton's equation's once yields momentum and integrating them twice yields positions for each atom. As a side note, it is possible to move atoms over a potential energy surface in a sequence of random steps. The method only needs a potential energy function.[20] This method is known as Metropolis Monte Carlo. Monte Carlo positions are generated stochastically so that a molecular configuration of R^n depends only on the previous configurations of the system in order generate positions.[20]

Again, the most straight forward molecular simulation method is molecular dynamics and its fundamental equation is Newton's second law Equation (2.1.4). Equation (2.1.4) is a differential equation so to solve it, there needs to be an integration algorithm, initial positions and boundary conditions. A well-known integration algorithm is the Verlet algorithm. All MD simulations assume that the positions, velocities, accelerations, and other higher order time derivatives of position can be approximated as Taylor series expansions[22]

$$r(t+\ \delta t) = r(t) +\ \delta t v(t) + \frac{1}{2}\delta t^2 a(t) + \frac{1}{6}\delta t^3 b(t) + \frac{1}{24}\delta t^4 c(t) +\ \ldots \tag{2.1.5}$$

$$v(t+\delta t) = v(t) + \delta t a(t) + \frac{1}{2}\delta t^2 b(t) + \frac{1}{6}\delta t^3 c(t) +\ \ldots \tag{2.1.6}$$

$$a(t+\delta t) = a(t) + \delta t b(t) + \frac{1}{2}\delta t^2 c(t) +\ \ldots \tag{2.1.7}$$

$$b(t+\delta t) = b(t) + \delta t c(t) +\ \ldots \tag{2.1.8}$$

Where the first derivative of the positions with respect to time is velocity, v, the second derivate of the positions with respect to time is acceleration, a, the third time derivative is b, and so on.

The Verlet algorithm is probably the most widely used method for integrating the equations of motion for molecular dynamic simulations, because the algorithm is straightforward and does not require large amounts of memory. It begins with two sets of positions $r(t) and\ r(t-\delta t)$ and accelerations, $a(t)$. The algorithm uses the positions and accelerations at time t, and the positions of the previous step, $r(t-\delta t)$, to calculate the new positions at time $t+\delta t, r(t+\delta t)$.[22] For this to work an initial state of the system must be given.

While using MD, the most important conditions in a molecular simulation are the initial positions and velocities of all atoms. The initial velocities are typically picked at random from a Maxwell-Boltzmann velocity distribution at some desired temperature.[20] There are several kinds of boundary conditions, for example vacuum, periodic, and stochastic boundary conditions. Vacuum boundary conditions should only be chosen when the system is in a vacuum or surrounded by a vacuum. For example, like the case of a small molecular cluster or a liquid droplet.[20] Periodic boundary conditions are better suited for our simulations.

Periodic boundary conditions are the most common boundary condition for solid systems. A parent system is surrounded with an infinitum number of copies of itself in all directions. If an atom leaves the parent cell its "periodic image" appears at the opposite side. Often the system is tested empirically, prior to actual calculations, by running simulations with increasing sizes to determine if the system feels any periodic effects.[20] Depending on how large the parent cell is, atomic interactions may occur across the boundary and within the parent cell, leading to invalid results. This can be corrected by simply increasing the size of the parent cell.

Although molecular forces and positions change with time, Newton's second law is time independent. The form $F_i = m\ddot{r}$ is invariant under time translations, thus there is some function of position and velocities with a value that is constant in time; this is called the Hamiltonian, H,[21]

$$H(r^n, p^n) = constant \tag{2.1.9}$$

$$p_i = m\dot{r}_i. \tag{2.1.10}$$

Where the in equation (2.1.9), the Hamiltonian is a function of position, r, and momentum, p. Then the momentum is defined as the total time derivative of position, equation (2.1.10). For an isolated system, the one conserved quantity is the total energy E.[21] It is the combined kinetic and potential energies of the molecules. Therefore, for an isolated system the total energy is the Hamiltonian for n spherical molecules, the Hamiltonian takes the form.[21]

$$H(r^n, p^n) = \frac{1}{2m}\sum_i p_i^2 + U(r^n) = E. \tag{2.1.11}$$

An important concept in computer simulation is the phase space. For a system containing N atoms, 6N values are required to define the state of the system (three coordinates per atom and three components of the momentum). Each combination of 3N positions and 3N momenta defines a point in the 6N-dimenstional phase space.[21] The way a system moves through phase space is governed by Hamilton's equations: [21] [22]

$$\frac{\partial H}{\partial p_i} = \frac{p_i}{m} = \dot{r}_i \tag{2.1.12}$$

$$\frac{\partial H}{\partial r_i} = -p_i \tag{2.1.13}$$

In molecular dynamics, the system generates a sequence of points in phase space that are connected in time. A molecular dynamics simulation performed in the micro-canonical, or constant-NVE, ensemble will sample phase space along a contour of constant energy.[22] Any conservative force can be written as the negative gradient of some potential function *U(r)*[22]

$$F_i = -\frac{\partial H}{\partial r_i} = -\frac{\partial U}{\partial r_i}. \tag{2.1.14}$$

Experiments are often performed under constant temperature T instead of constant energy E. This leads to other ensembles like NVT (canonical), NPT (isothermal-isobaric), and μVT (grand canonical). For NVT and NPT the number of atoms and the temperature are kept constant. NVT keeps the volume constant while NPT keeps the pressure constant. The μVT ensemble keeps the chemical potential, volume, and temperature constant.

In Newtonian dynamics, the motion is a response to an applied force, however in the Hamiltonian dynamics forces do not appear explicitly. Instead the motion occurs in such a way to conserve the Hamiltonian function.[21] To obtain the Hamiltonian equation of motion, the simulation must isolated system. If the system could exchange energy with its surroundings, then the Hamiltonian would contain additional terms to account for those interactions, thus meaning that the Hamiltonian is not the total energy of the system.[21] Therefore Hamiltonian would still be conserved, but not the total energy.

2.2 Embedded Atom Method

For molecular dynamics, lower symmetry and long-range strains generally found around defects and surfaces require techniques that can compute for large number of atoms. Thus, a model of a solid which is both accurate and computationally cheap is needed.[23] The use of empirical or semi empirical interatomic potentials make it possible to simulate atomic systems consisting of 10^7 to 10^8 atoms. This provides the ability to study problems such as plastic deformation, fracture, or atomic diffusion.[24] One of such empirical methods, is the embedded atom method (EAM), it is an approach based on density functional theory. The total energy of a monatomic system is generally represented as[24]

$$E_{tot} = \frac{1}{2}\sum_{ij} V(r_{ij}) + \sum_{i} F(\bar{\rho}_i) \tag{2.2.1}$$

$$\bar{\rho}_i = \sum_{j \neq i} \rho(r_{ij}) \tag{2.2.2}$$

Once the general form of the potential is chosen, the important issues become how to choose the database for fitting and how to parameterize and optimize the potential functions. Empirical potentials for monoatomic metals are typically fitted to experimental values of the equilibrium lattice parameter a_0, the cohesive energy E_0, three elastic constants, and the vacancy formation energy E_v^f.[24] This basic set of properties is often used along with planar fault energies, low index surface energies, and phonon frequencies.[24] Depending on the potentials chosen, the atomistic simulations are free to explore different atomic configurations that can be quite far away from the regions represented by the experimental data. An important property of potentials is the transferability, the accuracy of the potential over a range of configurations i.e. the types of simulations.

EAM potentials are usually construed by fitting experimental and/or first-principle data for a material at zero degrees Kelvin. It is not evident a priori that a potential fit to 0 K properties will be transferable to high temperatures or that it will be capable of reproducing the entire phase diagram of the system.[25] Folies et al.[23] defined EAM on the energy of each atom is computed from the energy required to embed the atom in the local electron density as provided by the atoms of the metal. This electron density is an approximate of atomic-electron densities.[23] They defined their total energy as

$$E_{tot} = \sum_i F_i(\rho_{hi}) + \frac{1}{2}\sum_i \sum_{j \neq i} \phi_{ij}(R_{ij}) \tag{2.2.3}$$

$$\rho_{hi} = \sum_{j \neq i} \rho_j^a(R_{ij}) \tag{2.2.4}$$

Foiles et al.[23] developed a consistent set of embedding functions and short-range repulsive pair interactions which are suitable to describe the FCC metals copper, silver, gold, nickel, lead, and platinum. While the parametric form for these potential functions may not be the best possible choice for a specific metal or alloy system, it is useful to have a common set of functions that provide a good description of a large set of metals and alloys. This facilitates the determination of trends over a range of metals or alloys.[23] The functions have been determined empirically by fitting the predicted results to the equilibrium density, sublimation energy, elastic constants, and vacancy formation energy of the pure metals as well as the heats of solution of the binary alloys.

The starting point of the EAM is the observation that the total-electron density in a metal is reasonably approximated by the linear superposition of contributions from the individual atoms. The electron density in the vicinity of each atom can then be expressed as a sum of the

density contributed by the atom plus the electron density from all the surrounding atoms. This latter contribution to the electron density is a slowly varying function of position.[23] By taking the simplification that this background electron density is a constant, the energy of this atom is the energy associated with the electron density of the atom plus the constant background density.

This defines an embedding energy as a function of the background electron density and the atomic species. The functions only give qualitatively correct calculation of the material's properties, so it is necessary to determine these functions empirically in order to obtain an accurate description. The information used in their empirical fits actually only determines the force, F_σ, and its first two derivatives for electron densities near the average host electron density, r_σ, of the bulk pure metals at equilibrium.[24]

There are alternative EAM potentials, for example Mishin et al.[24] developed their own set of potentials used for molecular dynamics. The Mishin potentials define the total energy of a monoatomic system similarly to equation (2.2.3)[245] and charge density similarly to equation (2.2.4)[25]. The Al and Ni potentials developed follow same form of the Folies potentials, but are fitted using experimental data for equilibrium lattice parameter, cohesive energy, elastic constants, and vacancy formation energies.[25] Others can include experimental properties from experiment like the surface energy, γ_s and the equation of state (EOS the crystal energy as a function of the lattice parameter a).[25]

The intrinsic shortcomings of EAM model is that although very successful in accounting for the nature of metallic bonding, the simple model is based on certain experimental approximations, which make it insufficient for many situations. For the case of bi-atomic systems Mishin et al.[25] also developed another potential following the same definition of energy in equation (2.2.3). This will aid in the study of metallic structure consisting of different types of

atoms. The drawbacks of older EAM potentials, like Foiles potentials, is that they are based on a small database of experimental properties and/ or a small number of fitting parameters, no tot mention the failure to use modern algorithms for multidimensional parameterization. Foiles potentials may be outdated, but they are fitted using similar experimental data[23]. For this reason, our calculations utilized the Foiles potentials.

The other EAM potentials lacked potentials of all three metals (silver, copper, and nickel). For consistency only one set of potentials must be used. Since potentials from different developers are parameterized differently, we cannot compare results obtained from different potential parameterizations.

2.3 Simulation Procedures

In this section, the description on how the results of the molecular dynamic calculations were performed will be discussed. The simulation package the molecular dynamic simulations were performed using LAMMPS[26] with Foiles potentials developed for copper, nickel, and silver. Again, the Foiles potentials were chosen over other potentials for the purpose of consistency.

The geometry of [1 1 1] oriented nanowires with circular cross-sections were generated with and without a (1 1 1) twin boundary. Periodic boundary conditions were imposed along the z axis (along the [111] direction) and shrink wrapped conditions were used in the x and y directions. The volume of the system was defined as

$$V = \pi \left(\frac{1}{2} D\right)^2 L,$$

(2.3.1)

Where D is the averaged diameter of the nanowire in the xy plane and L is the length of the nanowire.

The radial dependence simulations simulated nanowires with radii ranging from 20Angstroms (A) to 50A for all three metallic nanowires. Each model was thermally relaxed for 50,000 timesteps with constant NVT integration with Nose-Hoover thermostat. The timestep was set to 0.005 picoseconds. The nanowires were deformed in in the z direction by straining the simulation box at a constant engineering strain rate of 0.001 per picosecond at constant temperature of 300K for 200000 timesteps.

For the temperature dependence, radii of the nanowires were kept at 20 Angstroms for all three metals. Similarly, the timestep was set to 0.005 picoseconds. Each model was thermally relaxed for 50,000 timesteps with NVT integration with Nose-Hoover thermostat at 100K, 300K 500K, 800K, and 1100K. The nanowires underwent tensile deformation by straining the simulation box at a constant engineering strain rate of 0.001 per picosecond along the [1 1 1] direction for 200000 timesteps.

For silver and copper nanowires 100 ensembles were simulated and for nickel 160 ensembles were simulated. The average yielding stress was calculated as follows:

$$\sigma_j = \frac{\sum_i^N \sigma_i}{N} \tag{2.3.2}$$

Where $\sigma_j$is the average stress of a particular strain j, σ_i is the individual ensemble stress at a particular strain j, and N is the number of ensembels.

Chapter 3: Results

3.1 Radial dependences

This chapter will discuss the molecular dynamic results of silver, copper, and nickel nanowires to understand the effect twinning plans have on face centered cubic (FCC) structures. In this section molecular dynamic simulations were conduceted to varify any radial dependencies on the yielding stress of metalic nanowires. The nanowires radii range from 20 to 50 Angstroms(A). The molecular dynamic calculations for all nanowires were performed until an engineering strain of 0.1 was achieved.

Neighter the twinned or the un-twinned nanowires fractured, but a single yield point was achieved. Figure yielding stress verses radius displays the average yield points of 100 simulations for silver and copper and 200 simulations for nickel. The standard deviation,SD, of the yielding point was calucated as follows [27]:

$$SD = \sqrt{\frac{1}{N-1}\sum(x_i - \bar{x})^2}.$$

(3.1.1)

Where $\bar{x}$ is the averaged stress at the yielding point, N is the total number of simulations, x_i is the stress at the yielding point of each individual simulation. The more reliable measure of error is the standard deviation of the mean, SDM, defined as follows [27]:

$$SDM = \frac{SD}{\sqrt{N}}.$$

(3.1.2)

In our yielding results, we use the SDM to characterize the the uncertainty in the calculations. A complete table of standard deviations and standard deviation of the mean and any other error values can be seen in appendix B.

In the case of silver, the nanowire radii chosen were 20A, 30A, 40A, and 50A. The length of the nanowires were calculated as 7z, where z is the averaged equilibrium lattice length in the [111] direction for each radius of the silver nanowires. From figure 3.1.1, it is clear that silver nanowires with twinning planes yield later than their un-twinned counterparts. This means that the twinned nanowires can experience a larger tensile stress and still return to equilibrium position before yielding. As the radius of the nanowires increase the difference in yielding stress also increases.

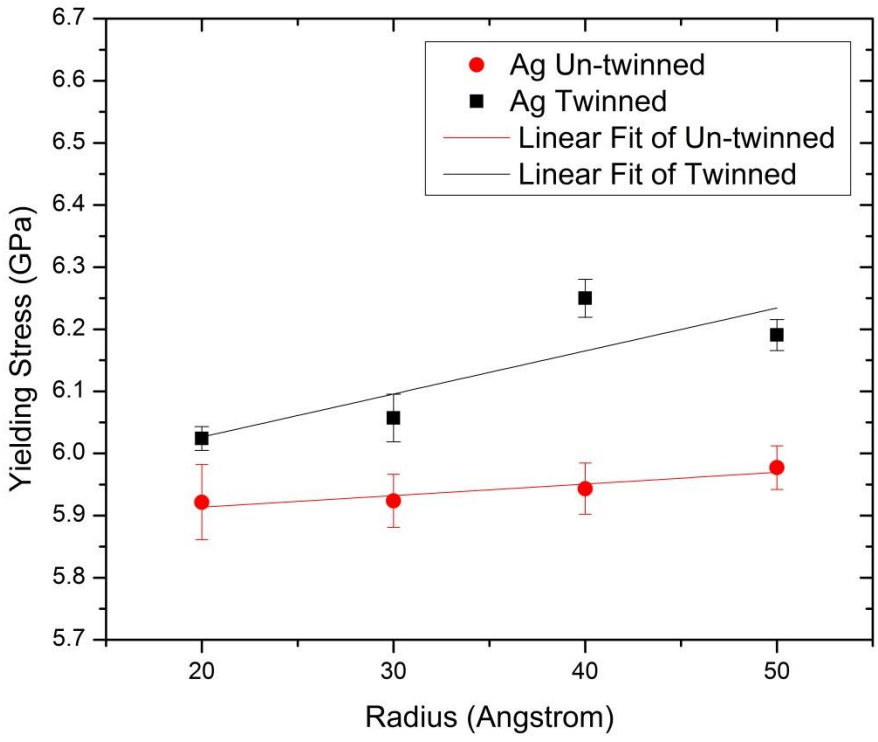

Figure 3.1.1: Yieling stress versus radius relation for silver nanowires. The yielding stress for twinned nanowires are denoted with red cirlces and standard deviation of means are shown as red error bars. The yielding stress for un-

twinned nanowires are denoted with black squrares and the standard deviation of means are shown as black error bars.

The difference in yielding stress σ_{diff}, is the difference between the twinned and untwinned nanowires of equal radius, calculated as follows:

$$\sigma_{diff} = \sigma_{twinned} - \sigma_{untwinned}.$$

(3.1.3)

Where $\sigma_{twinned}$ is the average yielding stress for twinned nanowires and $\sigma_{untwinned}$ is the average yielding stress for un-twinned nanowires. To estimate the uncertainty in the difference, only the highest and lowest probable values are needed. The highest probable value of σ_{diff} is[27]

$$\sigma_{diff} + (d\sigma_{twinned} + d\sigma_{untwinned}),$$

(3.1.4)

and the lowest probable value is[27]

$$\sigma_{diff} - (d\sigma_{twinned} + d\sigma_{untwinned}).$$

(3.1.5)

These are the upper and lower error bars in the yielding stress difference versus radius figures.

As the nanowire diameter increases, the difference in yielding stress also increases, as seen in figure 3.1.2, this displays the σ_{diff} relation with radius. The minimum difference in yielding stress for silver is 0.1GPa and the maximum difference in yielding stress is 0.4GPa. This suggests that as the radius of the nanowires increases, the harder the twinned nanowires

become. Thus, the strengthening effect of twinning planes, in silver nanowires, increase as the diameter increases. The strength gained can be shown my normalizing the yielding stress.

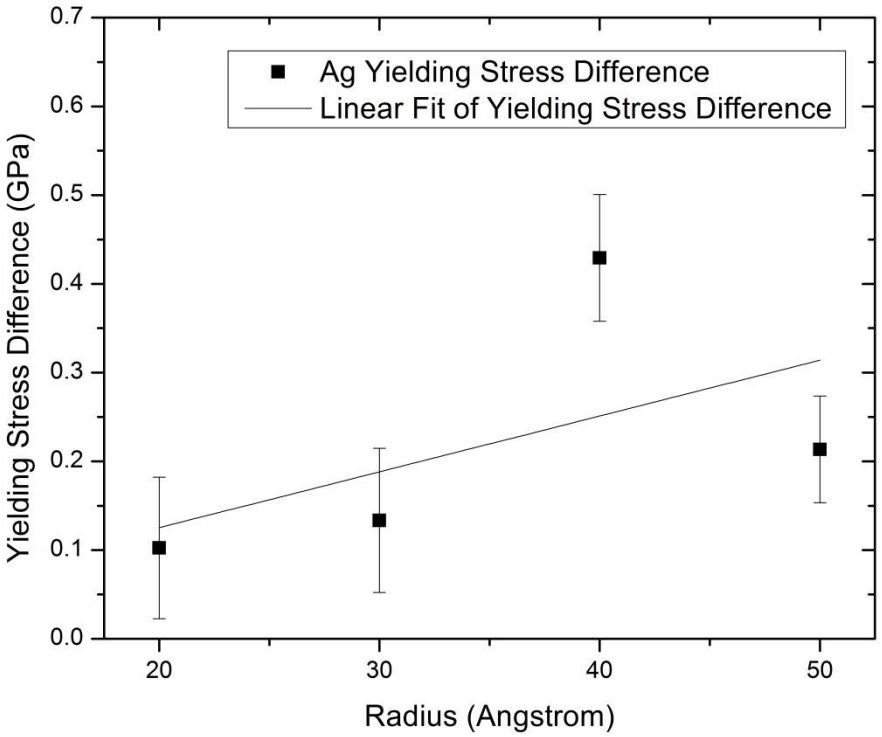

Figure 3.1.2: Difference in yielding stress verses radius relation for silver nanowires. The difference in yielding stress is between twinned and un-twinned nanowires of equal radius.

The normalized difference in yielding stress, or normalized stress σ_{norm}, is a measure of how much stronger the nanowires become by introducing twinning planes. A positive value indicates that strengthening occurs when growing twinning planes, while a negative value indicates weakening. The normalized stress is calculated as follows:

$$\sigma_{norm} = (\sigma_{twinned} - \sigma_{untwinned})/\sigma_{untwinned}. \tag{3.1.6}$$

Where $\sigma_{twinned}$ is the yielding stress of twinned nanowires and $\sigma_{untwinned}$ is the yield stress of un-twinned nanowires. The error of the normalized stress is calculated as follows:

$$d\sigma_{norm} = \frac{\sigma_{diff}}{\sigma_{untwinned}}\left(\frac{d\sigma_{twinned}+d\sigma_{untwinned}}{\sigma_{diff}} + \frac{d\sigma_{untwinned}}{\sigma_{untwinned}}\right). \tag{3.1.7}$$

This is simply the sum of the fractional uncertainties[27] in the numerator and denominator.

From figure 3.1.3, it is clear that as the nanowire radius increases the normalized stress increases, thus showing positive strengthening. The smallest increase in strength is 1.7% and the largest increase in strength is 5% for the silver nanowires. As the radius of the nanowires increases, the strength gain increase, which means that as the radius increases, the effect of the twinning planes becomes more significant.

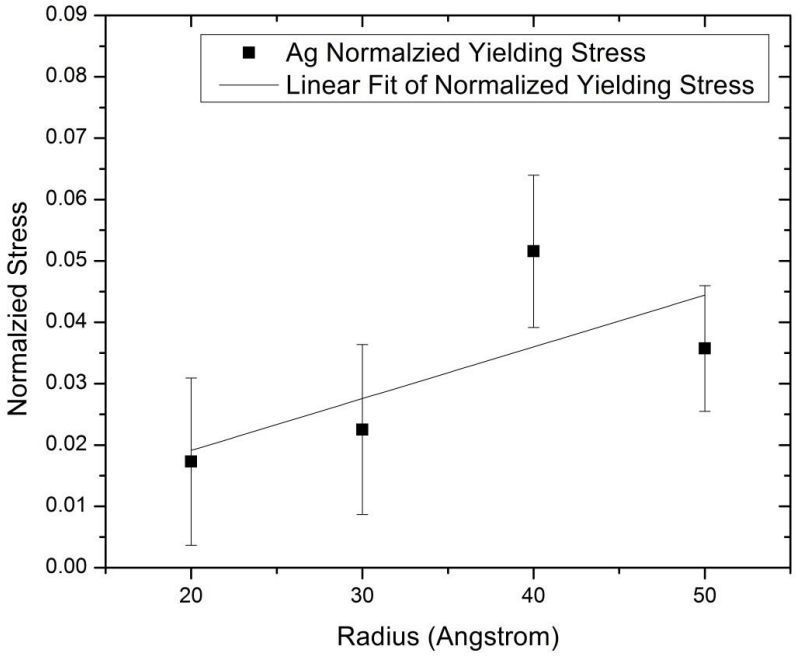

Figure 3.1.3: Normalized stress versus radius relation for silver nanowires.

The molecular dynamic simulations for copper nanowires were performed similarly to the silver nanowires, previously discussed. Again, during the straining process no fracturing of the nanowires was recorded. The radii used for copper are 20, 25, 30, 35, 40, and 45A. The length of the nanowires were calculated as 7z, where z is averaged equilibrium lattice spacing in the [111] direction.

Copper nanowires with twinning planes have greater yielding stresses than the untwined counterparts. The radial dependence on yielding stress can be seen in figure 3.1.4, it appears that as the radius increases, the yielding stress decreases for both the twinned and un-twinned copper nanowires. Alternatively, one could argue that the average yielding stress remains constant as the radius increases. From figure 3.1.4, by examining the error bars, the yielding stress may be overestimated for the un-twinned nanowire with radius 25A. Also the yielding stress for the twinned nanowire with radius 35A may be underestimated. If the yielding points were lower or higher, within the uncertainty, then the radial relation with yielding stress would appear more constant for both types of nanowires. Regardless, the yielding stress difference appears to be constant with increasing radii, this can be better viewed by plotting a yielding stress difference to radius plot.

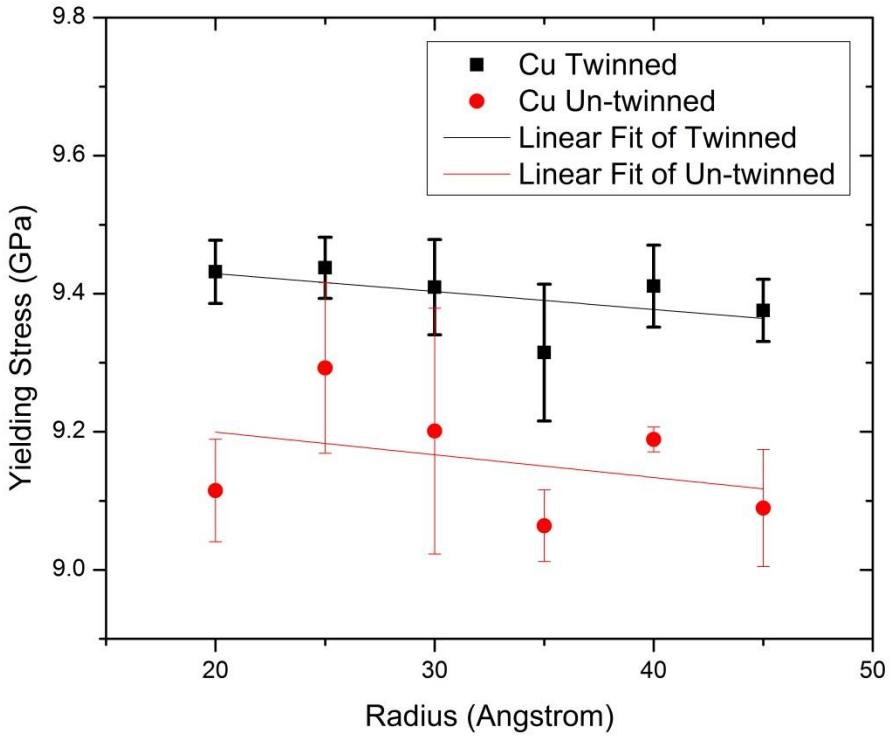

Figure 3.1.4: Yieling stress versus radius relation for copper nanowires. The yielding stress for twinned nanowires are denoted with red cirlces and standard deviationis are shown as red error bars. The yielding stress for un-twinned nanowires are denoted with black squrares and the standard deviations are shown as black error bars.

The radial relationship on the difference in yielding stress for copper nanowires is shown in figure 3.1.5. The radius does not appear to affect the difference in yielding stress for copper nanowires. Once could argue that the trend of yielding stress difference increases with radius, but by examining the uncertainty in the difference between the 25A nanowires, it seems that the difference may be underestimated. From figure 3.1.5, it appears that by introducing twinning planes to copper nanowires, the nanowires harden the same for any radius, which means that the nanowires of any radius gain an equal amount of strength.

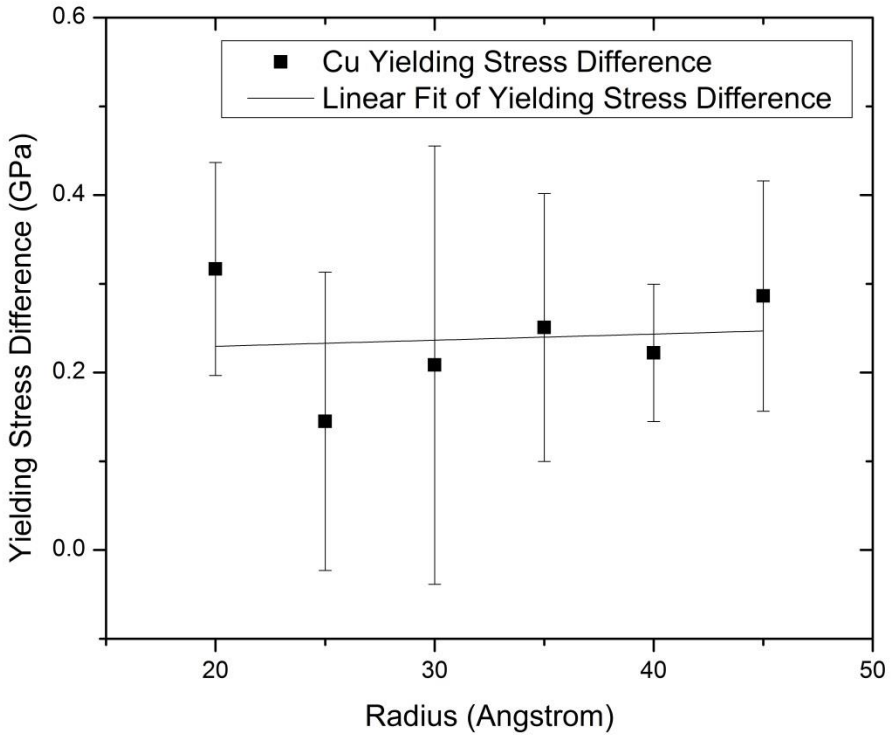

Figure 3.1.5: Difference in yielding stress verses radius relation for copper nanowires. The difference in yielding stress is between twinned and un-twinned nanowires of equal radius.

Using equation (3.1.6) to find the normalized yielding stress, figure 3.1.6 shows the radial dependence on the normalized yielding stress for copper nanowires. Again, one could argue that the trend appears to be increasing, but within our estimated uncertainty, the yielding stress appears constant. From figure 3.1.6, the normalized yielding stress appears to be constant with changing radii, thus suggesting that the strength gain by adding twinning planes to copper nanowires is independent of the size of the nanowire.

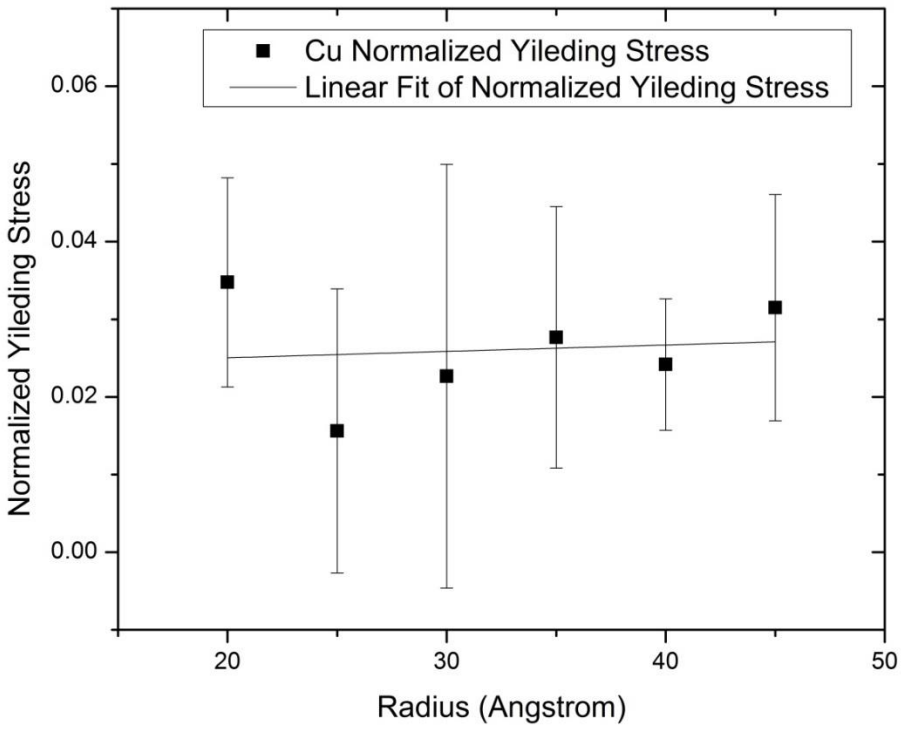

Figure 3.1.6: Normalized stress versus radius relation for copper nanowires.

In comparison, the maximum strength grained is 3.5% for copper nanowires and 5% for silver nanowires. From our calculations, growing smaller silver nanowires with twinning planes diminishes the strengthening effects in silver nanowires. Growing smaller copper nanowires with twinning planes won't diminish the strengthening effects of copper nanowires, at least for nanowires from 20 – 50A. For applications requiring smaller nanowires, copper appears to be a better choice in material.

The molecular dynamic simulations for nickel nanowires were performed under the same conditions as the copper nanowires and with the same radii. The yielding stress versus radius of nickel nanowires, shown in figure 3.1.7, shows the nickel nanowires with twinning planes

yielding later than the un-twinned nanowires. The yielding stress of twinned nanowires increases as the radius increases. The un-twinned nanowires appear to have an opposite trend, the yielding stress decreases as the radius increases. One could argue that the yielding stress for the 40A un-twinned nanowire may be underestimated within its error bars. Regardless, the difference in yielding stress grows as the diameter becomes larger.

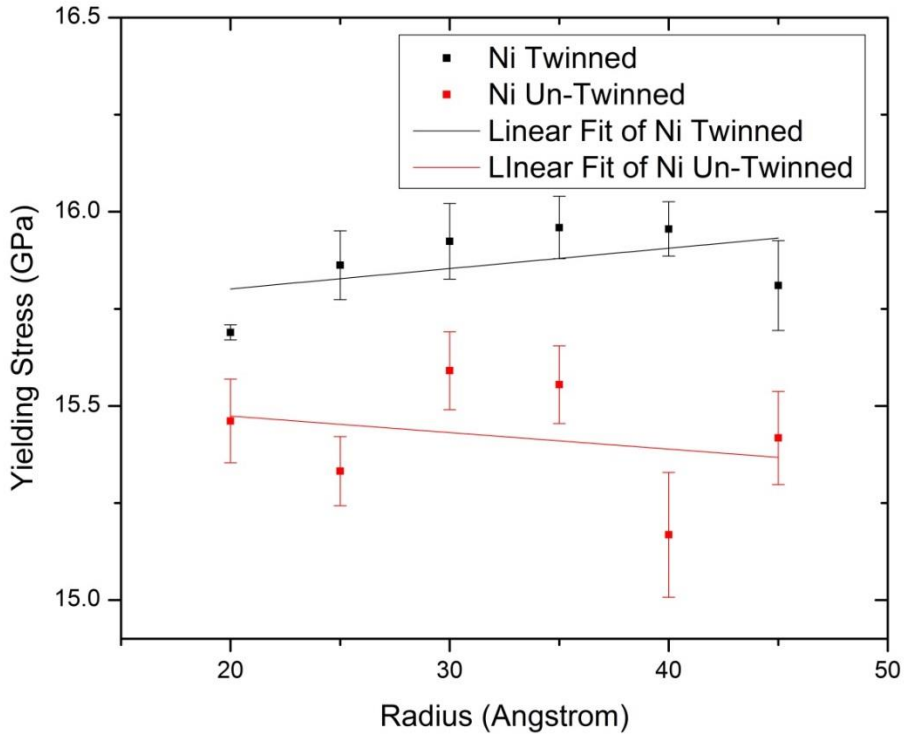

Figure 3.1.7: Yieling stress versus radius relation for nickel nanowires. The yielding stress for twinned nanowires are denoted with red cirlces and standard deviationis are shown as red error bars. The yielding stress for un-twinned nanowires are denoted with black squrares and the standard deviations are shown as black error bars.

For nickel nanowires, the difference in yielding stress increases as the radius increases, as shown in figure 3.1.8. This suggests that the twinning planes harden nickel nanowires as the radius increases. The error bars for the yielding points of 25A and 40A radius nanowires

suggests that the averaged yielding stress may be overestimated. The strength gained by introducing twinning planes appears to grow as the radius increases.

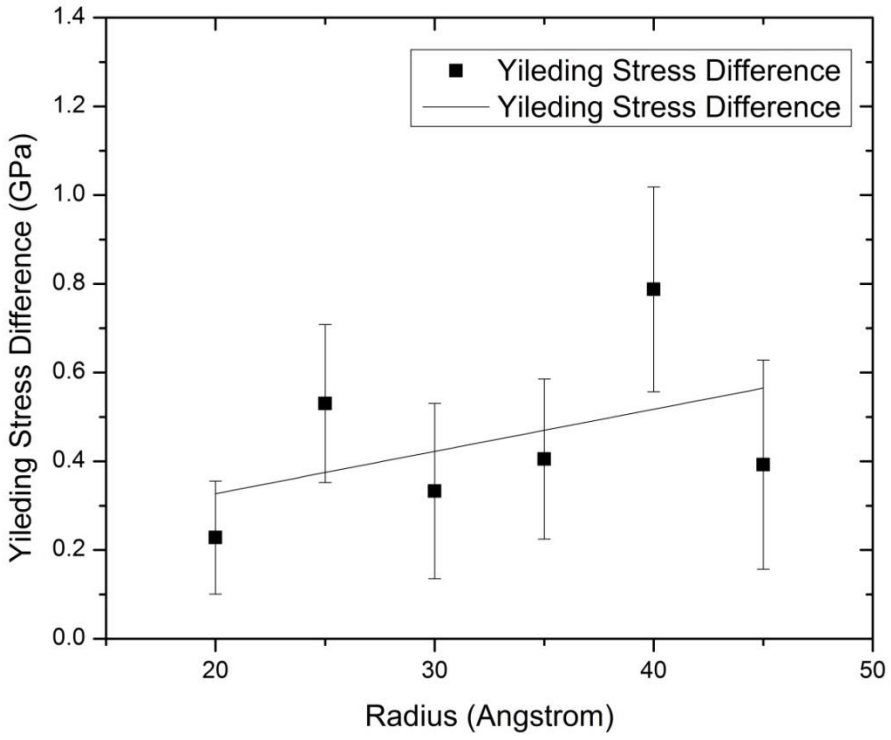

Figure 3.1.8: Difference in yielding stress verses radius relation for nickel nanowires. The difference in yielding stress is between twinned and un-twinned nanowires of equal radius.

The normalized stress is again calculated using equation (3.1.6) and the radial dependence is shown in figure (3.1.9). As shown, the normalized stress increases as the nanowire radius increases. Again, the error bars for the 25A and 40A radius show that there is a probability the average yielding stress may be overestimated. However, this does not affect the increasing trend the normalized stress has with the radius. Thus, the strengthening effects are greater for nanowires with larger radii.

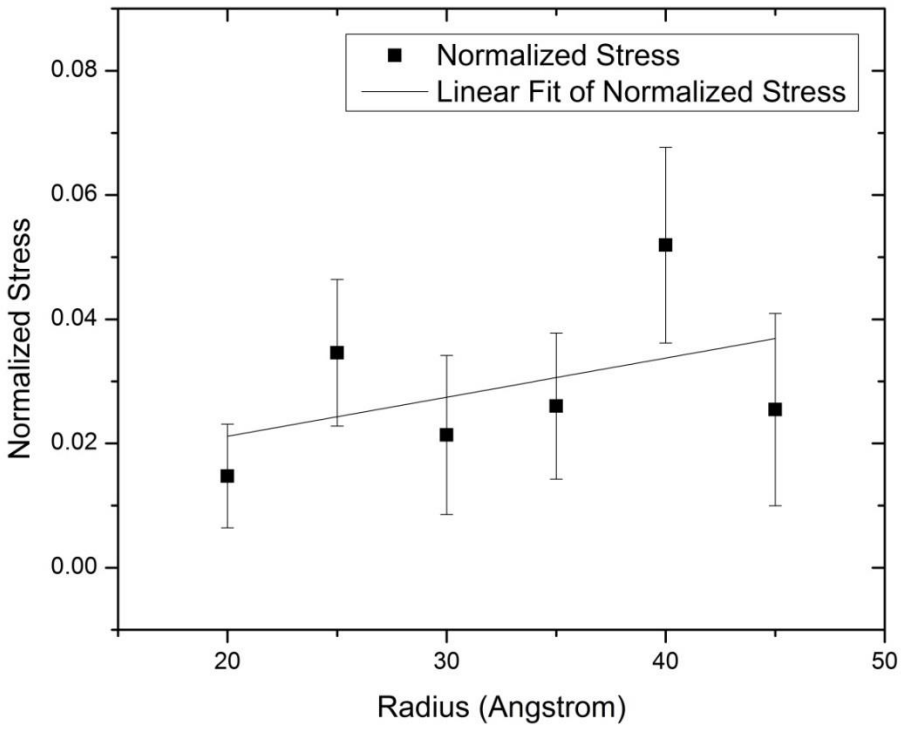

Figure 3.1.9: Normalized stress versus radius relation for nickel nanowires.

The nickel nanowires behave similarly to the silver nanowires, because for both as the radius increases the yielding stress difference increases. This suggests that twinning planes have more of a strengthening effect for those larger nanowires, ~5%, and that for smaller nanowires the strengthening effects become minor, ~1%. In contrast, copper nanowires maintain a constant strength gain, ~2.5%, independent of nanowire size. Of course these results are for nanowires ranging from 20A to 50A in radius.

It is possible to extrapolate values of larger nanowires using the data. As shown in the above figure, the linear trend lines can be used to extrapolate values of yielding stress for larger nanowires. A sample of extrapolated data points are shown in appendix C.

In comparison, from the previous figures; figure 3.1.1, figure 3.1.4, and figure 3.1.7, there is a general agreement that the twinned nanowires yield later than the un-twinned nanowires. The results suggest that twinned nanowires have a longer elastic region, so after loading the nanowires will return to their un-stretched equilibrium states. Our results of twinning planes agree with those of Zhang[1] and Cao[15] which further suggests that twinned boundaries interrupt the glide of dislocations, thus promoting strengthening.

The radial dependence of the both silver nanowires and nickel nanowires with twinning planes, contradict the inverse relationship described by Cao[15], Jing[3], and Lucas[5]. The inverse relationship states that the yielding stress increases as the diameter decreases, but as seen from figure 3.1.1 both the twinned and un-twinned silver nanowires yield increase as the radius increases. From figure 3.1.7, the twinned nickel nanowire shows the yielding stress increases as the radius increases. One could argue that both copper nanowires and the un-twinned nickel nanowires follow the inverse relationship, but a constant trend line can be drawn within their error bars suggesting those nanowires to have an independent relationship to the radius.

The yielding relationship with diameter may not follow experimental or other calculated results, because our nanowires are smaller than literature values. Remember, our simulated nanowires had radii ranging from 20A to 50A. The yielding relationship, described by Cao15[15], Jing[5], and Lucas[3], were formed for nanowires with diameters with radii ranging from 50-200nm. Those nanowires are 10 to 100 times larger than the nanowires we simulated, so the inverse relationship may be applicable to our results.

From figures 3.1.2 and 3.1.8, the yielding stress difference grows as the nanowire diameter increases in the case of silver and nickel, suggesting that there is a size dependence on

hardening. For the case of copper the hardening was independent of the size of the nanowires, shown in figure 3.1.5. This suggests that the copper nanowires have no size dependence on hardening. The amount of strength gained was measured using the normalized stress.

The normalized stress increases as the radius increases, as seen in figures 3.1.3 and 3.1.9. This implies that as the radius of silver and nickel nanowires increases, the twinned nanowires will have a greater gain in strength. The best gain in strength is about 5%. In the case of copper, figure 3.1.6 shows that the strength gained is independent to the size of the nanowire. To our knowledge, there have been no known reports on a normalized stress relationship with respect to diameter in the literature.

3.2 Temperature Dependence

This section will discuss the effect temperature has on the yielding stress of silver, copper, and nickel nanowires. In the previous section, each nanowire was simulated under room temperature, 300K only. The results of this section simulated nanowires under temperatures of 100K, 300K, 500K, 800K, and 1100K. For this study, the nanowires all have radius of 20A.

For the silver nanowires, the simulations results exclude the values at 1100k because the nanowires melted. For bulk silver, the melting point is 1234.9K[28]. Figure 3.2.1 shows the relationship temperature has on the yielding stress. The silver nanowires with twinning planes always yield later than the un-twinned nanowires. As the temperature increased, both the twinned and un-twinned nanowires yield at lower stresses. Thus the colder the nanowire, the harder it becomes. From figure 3.2.1, the difference in yielding stress appears to be constant.

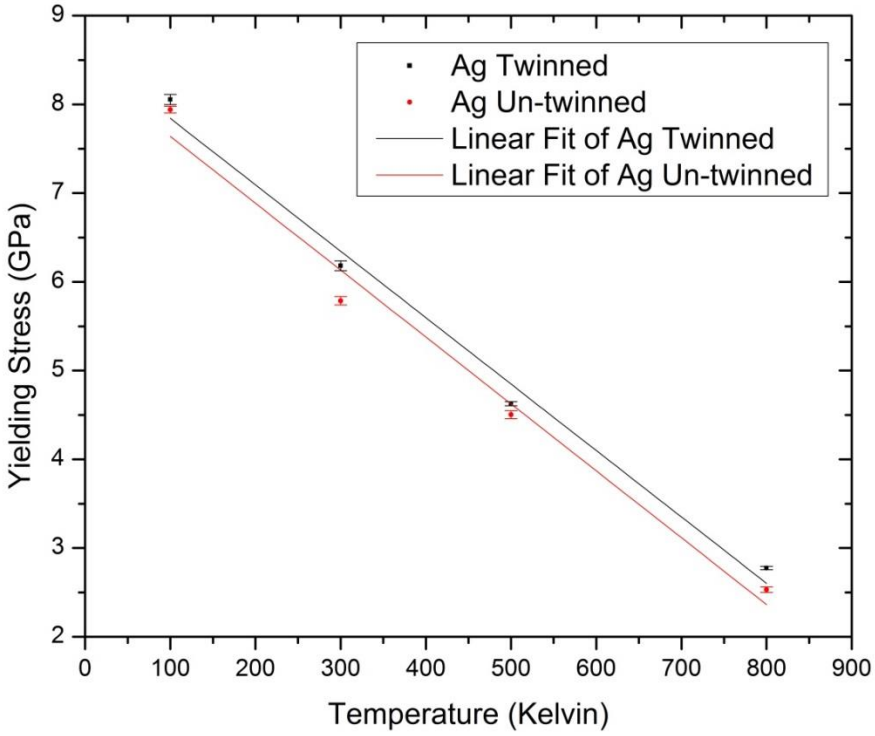

Figure 3.2.1: Yielding stress versus temperature dependence for silver nanowires. The yieling stress for twinned nanowires are marked as black squares and the standard deviation of mean marked as black error bars. The yeilding stress for un-twinned nanowires are marked as red circles and the standard deviation of mean marked as red error bars.

The difference in yielding stress appears constant, as shown in figure 3.2.2. The average difference in yield strength is 0.2GPa. One could argue that the difference in yielding stress increases with temperature, as shown with the linear trend line in figure 3.2.2. This would mean that, twinning planes make the nanowires harder than the un-twinned nanowires as the temperature increases. However, the uncertainty of the 300K yield point does not suggest that it is overestimated nor should it be lower than the 0.3GPa. Therefore we must conclude that the difference in yielding stress does not depend on temperature.

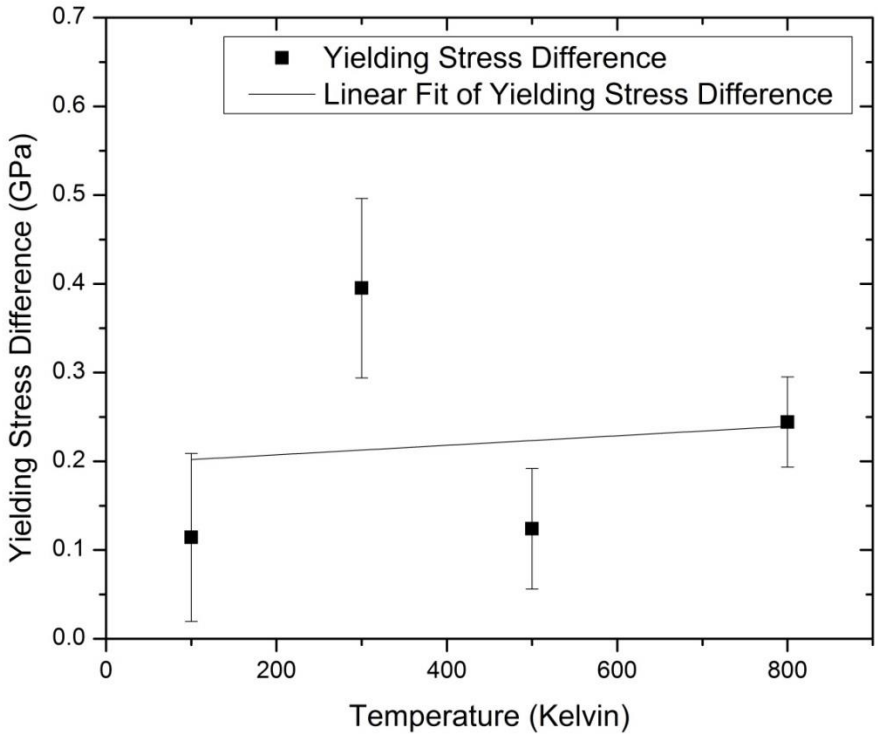

Figure 3.2.2: The difference in yielding stress versus temperature of silver nanowires. The error propagations are labeled as black error bars.

The strength gained by introducing twinning planes can be shown by normalizing the yielding stress. The normalized stress is calculated from equation (3.17). Figure 3.2.3 shows the normalized stress of silver nanowires versus temperature. The normalized stress increases as temperature increases. This means that the twinned nanowires do not soften as quickly as the un-twinned nanowires as the temperature increases. Thus the twinning planes have more of a strengthen effect at higher temperatures.

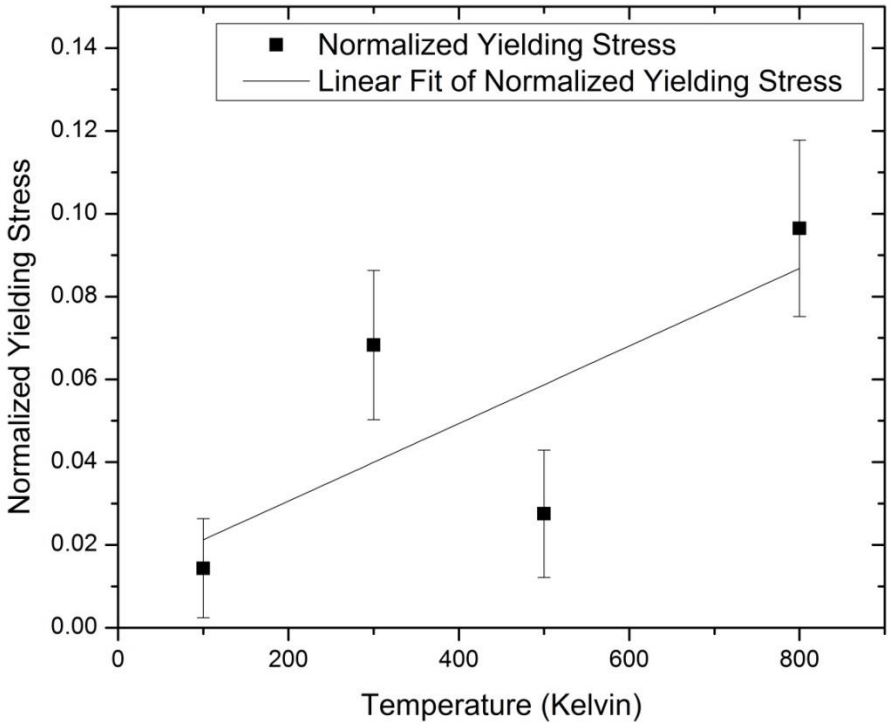

Figure 3.2.3: Normalized stress versus temperature dependence of silver nanowires. The error prorogations are labeled as black error bars.

The copper nanowires underwent the same conditions as the silver nanowires. For copper, the nanowires did not melt at 1100K like the silver nanowires. The melting point for bulk copper is 1357.8[28]. Figure 3.2.4 shows the relationship that the temperature has on the yielding stress of both twinned and un-twinned copper nanowires. When the nanowires are 100K, the un-twinned nanowires yield later than the twinned nanowires, thus suggesting that twinning planes do not strengthen copper nanowires at 100K. We do not have an explanation for this.

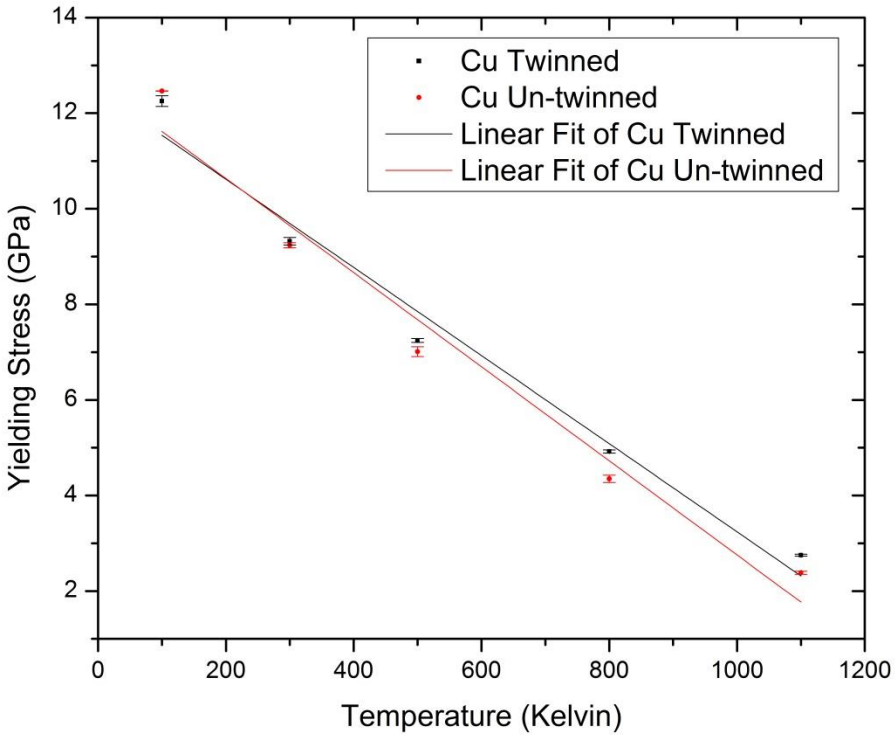

Figure 3.2.4: Yielding stress versus temperature dependence for copper nanowires. The yieling stress for twinned nanowires are marked as black squares and the standard deviation of mean marked as black error bars. The yeilding stress for un-twinned nanowires are marked as red circles and the standard deviation of mean marked as red error bars.

Although it appears that when the nanowires are 100K, the un-twinned nanowires are stronger, as temperature increases the twinned nanowires yield later than the un-twinned counterparts. The smallest difference is 0.08GPa and the largest difference is 0.6GPa. The difference in yielding stress increases as the temperature increases, as shown in figure 3.2.5. This relation shows that twinned copper nanowires soften slower than un-twinned nanowires as the temperature increases. Thus as the temperature increases the amount of strength gained also increases.

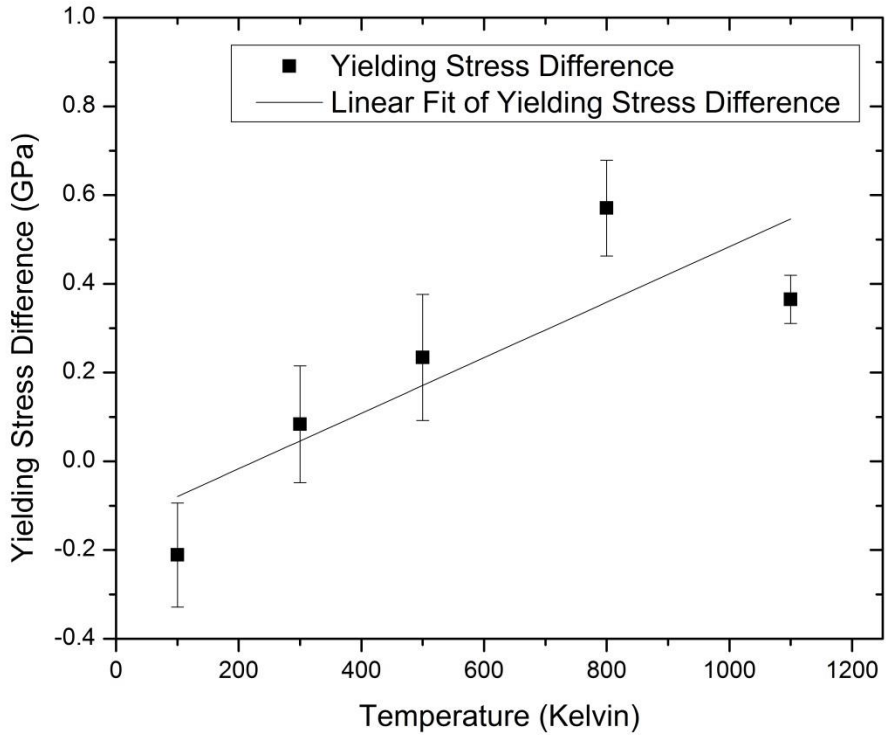

Figure 3.2.5: The difference in yielding stress versus temperature of copper nanowires. The error propagations are labeled as black error bars.

The normalized stress relation with temperature shows how much stronger the nanowires with twinning planes are compared to the un-twinned counterparts. Similarly, the normalized stress is calculated using equation (3.1.6). From figure 3.2.6 the normalized stress versus temperature results can be seen. The maximum strength gain by adding twinning planes is 15.3%. As the temperature increases, the normalized stress for copper also increases. Thus, as the temperature is increasing the strength gained is also increasing. For copper nanowires, twinning planes strengthen the nanowires prior to melting.

In comparison, silver nanowires melt earlier than copper nanowires and the introduction of twinning planes appears to only strengthen the silver nanowires by 10% prior to melting.

Copper has a higher melting point and prior to melting are 15% stronger than the un-twinned nanowires. By adding twinning planes, copper nanowires perform mechanically better than silver nanowires.

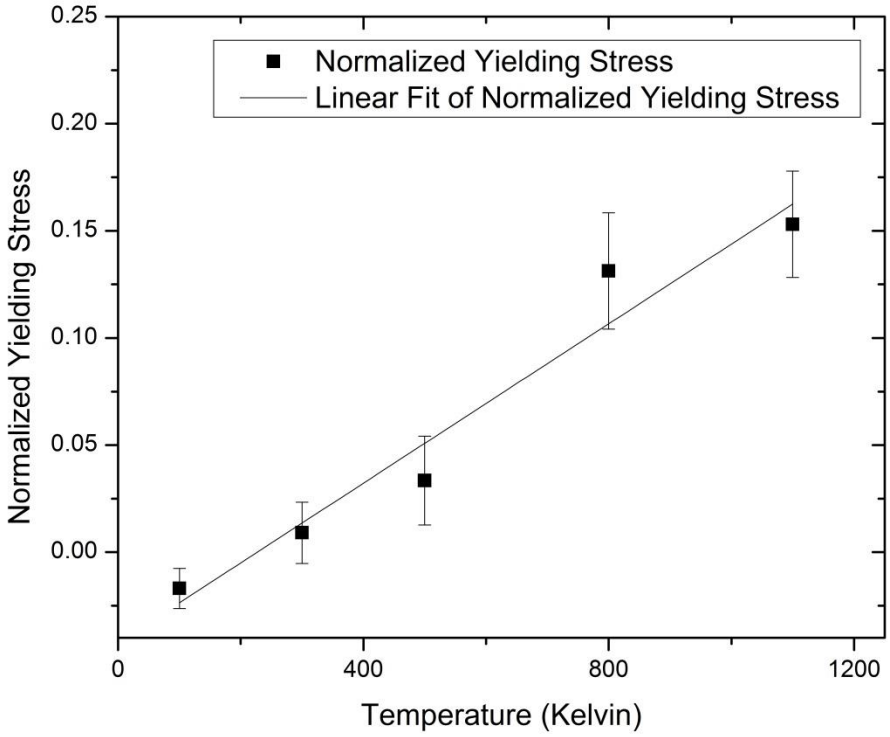

Figure 3.2.6: Normalized stress versus temperature dependence of copper nanowires. The error prorogations are labeled as black error bars.

The molecular dynamic simulations for nickel followed the same procedures as silver and copper. Similarly to copper, when the nanowires are simulated at 100K the un-twinned nanowires yield later than the twinned nanowires. The yielding stress relationship with temperature is shown in figure 3.2.7. As the temperature of the nanowires is 300K or greater, the yielding stress for the twinned nanowires is greater than the un-twinned counterparts. From

figure 5.2.7, both twinned and un-twinned nanowires decrease in yielding stress as temperature increases. The difference in yielding stress increases, the temperature increases.

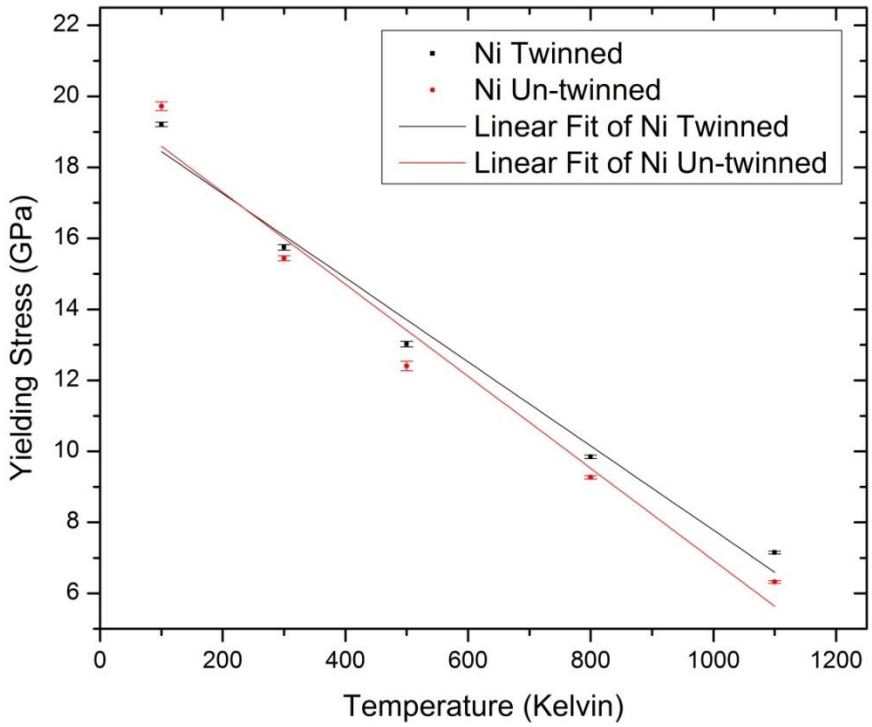

Figure 3.2.7: Yielding stress versus temperature dependence for nickel nanowires. The yieling stress for twinned nanowires are marked as black squares and the standard deviation of mean marked as black error bars. The yeilding stress for un-twinned nanowires are marked as red circles and the standard deviation of mean marked as red error bars.

The difference in yield stress with respect to temperature can be seen in figure 3.2.8. The maximum difference in yield stress is 0.8261GPa and the minimum difference in yield stress is 0.3058GPa, the difference in yield strength increases. This means that when the nickel nanowires are heated, the twinned nanowires soften slower than the un-twinned nanowires. Since difference grows as temperature increases, for higher temperatures the strengthening effect is greater.

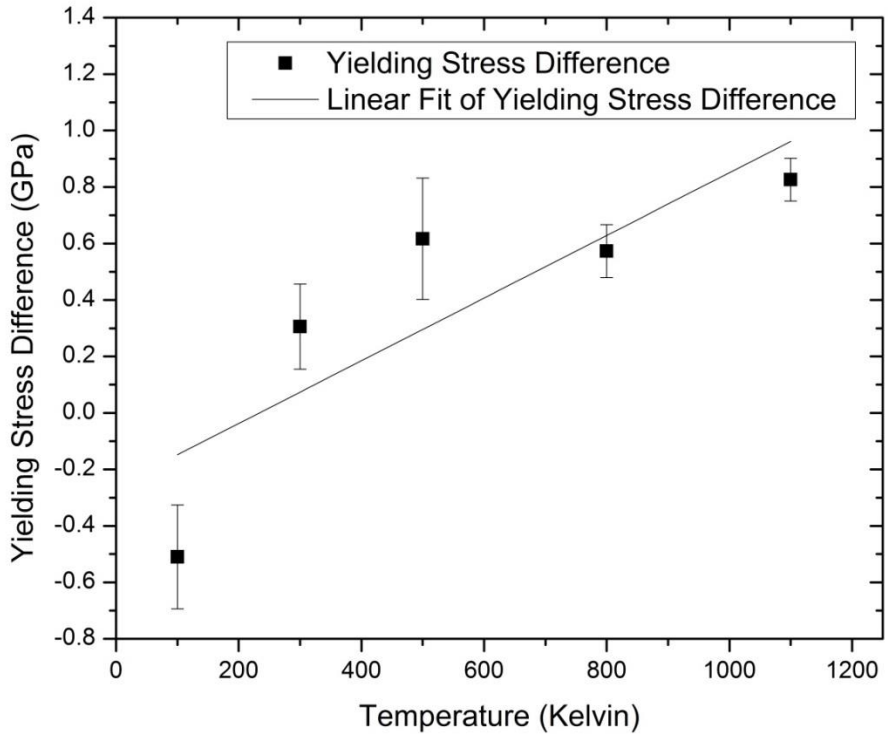

Figure 3.2.8: The difference in yielding stress versus temperature of silver nanowires. The error propagations are labeled as black error bars.

Similarly, the strengthening effect can be shown by normalizing the stress using equation (3.1.6). The normalized stress for nickel with respect to temperature can be seen in figure 3.2.9. From figure 5.2.9, as the temperature increase, the normalized stress increases. The greatest strength gained is 13.1% at 1100K. Thus when nickel nanowires are heated the stronger the effect twinning planes have on the yielding stress of nickel nanowires.

From figures 3.2.2 and 3.2.3, copper and nickel nanowires with twinning planes will benefit the most by growing twinning planes. The normalized stress prior to melting is about 0.18. This means that twinned nanowires will be 18% stronger than the un-twinned counterpart. Similarly, in the previous section, section 3.1, the yielding stress prior to melting can be

extrapolated using our data. Some examples of extrapolated values for the temperature dependence can be seen in appendix C.

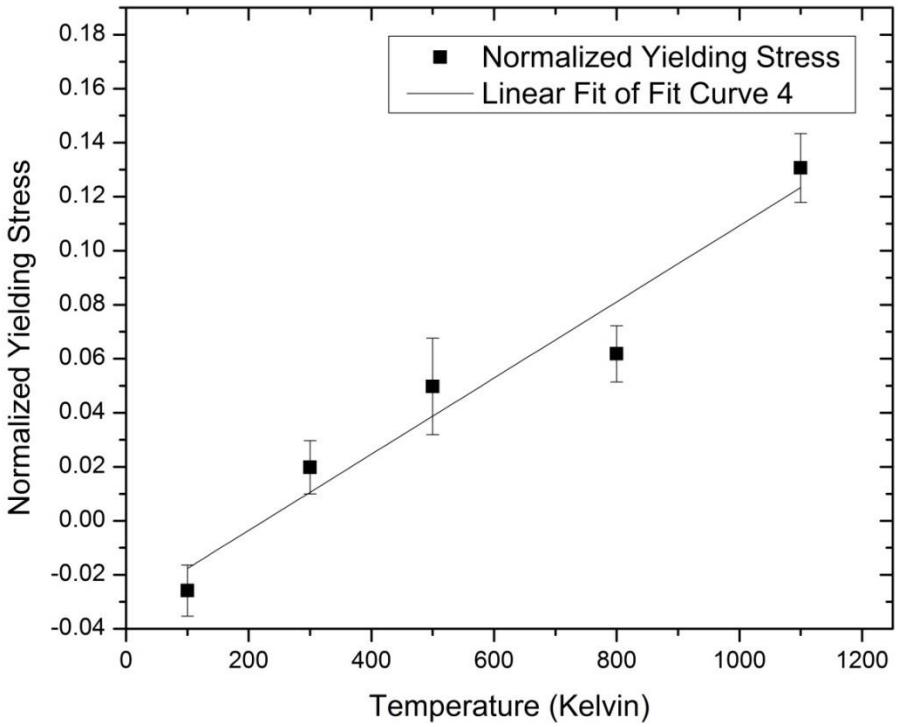

Figure 3.2.9: Normalized stress versus temperature dependence of nickel nanowires. The error prorogations are labeled as black error bars.

A clear trend appears for all metals as temperature increases, the yielding stress decreases as temperature increases. Our results agree with the work of Cao et al.[19] as the temperature decreases the yielding stress increases. In case of silver, the hardening effect is independent of temperature, but for nickel and silver as temperature increases the nanowires become harder. All three metals show that prior to melting the strength gained because of twinning planes becomes significant, 10% for silver, 15% for copper, and 13% for nickel. From a mechanical point of

view twinning planes have a large impact on strengthening prior to melting. To our knowledge there have been no reports of the temperature dependence on the normalized stress.

6.0 Conclusion

The purpose for these molecular dynamic simulations was to better understand the effects twinning planes had on the strength of metallic nanowires. From the radial results, a general trend can be made by introducing twinning planes, twinning planes harden nanowires. As the radius increased for silver and nickel, the difference in yielding stress increased. This suggested that for larger nanowires twinning planes better strengthen them. For copper nanowires, the hardening caused by the twinning planes was independent of the size of the nanowires.

The normalized stress increased as the silver and nickel nanowires increased in size. This means that by introducing twinning planes into the nanowires, the larger nanowires will have a greater gain in strength. The strength gained in copper nanowires is independent of its size, in applications that require smaller nanowires copper appears to be the better choice. Since the strengthening effects do not decrease with size, like silver or nickel, copper would be the better choice for adding twinning planes.

From the temperature trials a general trend can also be made for the normalized stress. As the temperature of the wires increased, the normalized stress also increased. This means that the twinning planes strengthen the nanowires at higher temperatures. Physically, metallic nanowires with twinning planes are harder than the un-twinned nanowires as temperature increases prior to melting.

In conclusion, our simulations show that twinning planes strengthen metallic nanowires. The amount of strength gain can vary for silver and nickel nanowires while for copper the strength gained appears constant. For higher temperatures twinning planes make nanowires soften slower than un-twinned nanowires and the strength gain near the melting point greater than 10%. This work hopes to influence the future of nano-science and technology by providing insight to the mechanical properties of silver, copper, and nickel nanowires.

Appendix A

The section will describe the basic definitions for stress, strain, yielding stress prior to the literature review. This chapter can be skipped; the importance of this chapter is to define mechanical behaviors and plastic behaviors for the reader. Stress is defined as the amount of force, F, per unit area[29]. True stress, σ, is defined in terms of the current area, A

$$\sigma = \frac{F}{A} \tag{A.1}$$

Nominal or engineering stress, S, in a tension or compression test is defined in terms of the original area A_0[29],

$$S = \frac{F}{A_0} \tag{A.2}$$

Strain describes the amount of deformation a material has undergone[29]. An increment of true strain, dε, is defined in terms of the length, L, as[29],

$$d\varepsilon = \frac{dL}{L}. \tag{A.3}$$

True strain is express as[29]

$$\varepsilon = \ln\left(\frac{L}{L_0}\right). \tag{A.4}$$

Engineering or nominal strain, e, is defined as[29]

$$e = \frac{\Delta L}{L_0}. \tag{A.5}$$

For small deformations, $e \approx \varepsilon$ and $S = \sigma$

When applying a force on the material, the loading process, the material will compress, stretch, or bend[29]. If the deformation exceeds a critical amount, the material will not return to its original shape. The material has yielded and deformed plastically. The behavior is frequently characterized by the engineering stress-strain curve in tension, similar to figure A.2.1. [29] It is possible to define and elastic limit as the stress at which the very first plastic deformation occurs and a proportional limit as the stress at which stress is no longer proportional to strain.

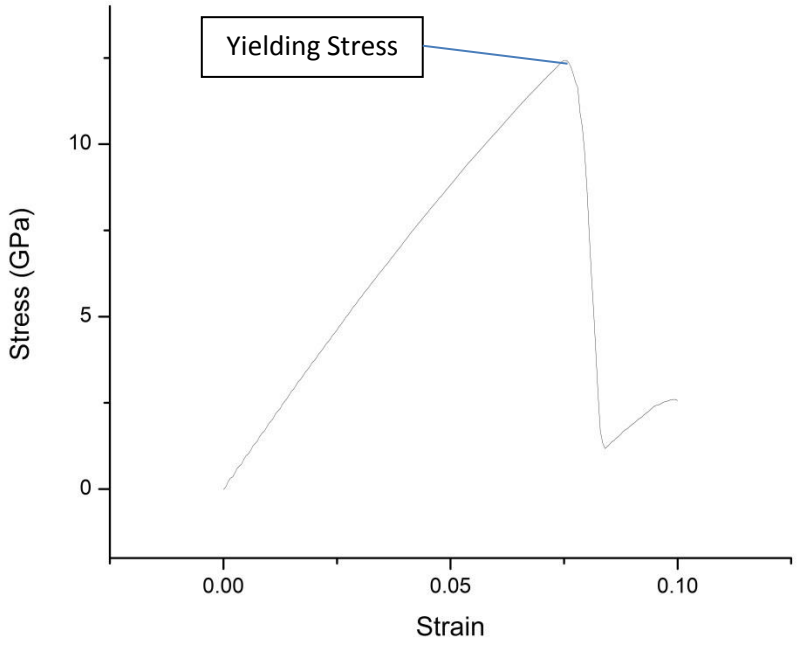

Figure A.1: Calculated stress strain curve of copper nanowires under tensile stress.

An initial drop of stress occurs after the yielding for a few materials. The upper yield strength is defined as the stress the first maximum and the lower yield strength are defined as the level of the plateau following initial yielding. The highest engineering stress is called the tensile strength or ultimate strength.

If a material is ductile, the tensile strength is reached before the material breaks the tensile strength corresponds to the point at which the deformation localized into a neck. For less ductile materials, fracture occurs before necking and in brittle materials before yielding[29], so the tensile strength is the fracture strength.

The ductility of a material describes the amount of deformation before fracture in a tension test.[29] There are two common measure of ductility. One measure is the percent elongation

$$\%El = \frac{(L_f - L_0)}{L_0} * 100\%,$$

(A.2.1)

and the other is the percent reduction of area

$$\%RA = \frac{A_0 - A_f}{A_0} * 100\%.$$

(A.2.2)

The percent reduction of area is a better measure of ductility because the percent elongation is both the uniform elongation before necking and the elongation during necking; which depends on the specimen's diameter. Tensile specimens with large length to diameter ratios have lower percent elongation than those with low length to diameter ratios[29].

The twinned boundaries behave similarly to grain boundaries. They are physical obstacles to deformation, so materials with finer grain sizes tend to have higher yield strengths. The Hall-Petch equation relates yield strength, σ_y, to the intercept grain size[29]:

$$\sigma_y = \sigma_0 + K_y d^{-1/2},$$

(A.2.3)

Where σ_0 and K_y are constants and d is the average grain diameter[29]. The grain boundaries impede slipping. Slips, or dislocations, are the primary mechanism by which plastic deformation occurs. Slip is the sliding of atomic planes over each other. The planes on which slip occurs and the direction of slip are crystallographic[29]. In metals, the planes on which slip occurs are the closest-packed planes, and the direction of the slip is the directions with shortest repeat distance.

Appendix B

Table B.1: Radial dependence results for silver nanowires. This table displays the difference in yielding stress, σ_{diff}, the error in calculating the difference using the standard deviation, $\delta\sigma_{diffSD}$, the error in calculating the difference using the standard deviation of the mean, , $\delta\sigma_{diffSDM}$, the normalized yielding stress,σ_{norm}, the error in calculating the normalized yielding stress using the standard deviation, $\delta\sigma_{normSD}$, and the error in calculating the normalized yielding stress using the standard deviation of the mean,$\delta\sigma_{normSDM}$.

Radius (A)	σ_{diff} (GPa)	$\delta\sigma_{diffSD}$ (GPa)	$\delta\sigma_{diffSDM}$ (GPa)	σ_{norm}	$\delta\sigma_{normSD}$	$\delta\sigma_{normSDM}$
20	0.10	0.80	0.08	0.02	0.14	0.01
30	0.13	0.81	0.08	0.02	0.14	0.01
40	0.31	0.72	0.07	0.05	0.12	0.01
50	0.21	0.60	0.06	0.04	0.10	0.01

Table B.2: Radial dependence results for silver nanowires. This table displays the yielding stress of un-twinned, $\sigma_{untwinned}$, the standard deviation of the un-twinned, $SD_{untwinn}$, the standard deviation of the mean of the un-twinned, SDM_{untwin}, the yielding stress of twinned nanowires,$\sigma_{twinned}$, the standard deviation of the twinned nanowires,SD_{twin} , and the standard deviation of the mean for the twinned yielding stress, SDM_{twin}.

Radius (A)	$\sigma_{untwinned}$ (GPa)	$SD_{untwinn}$ (GPa)	SDM_{untwin} (GPa)	$\sigma_{twinned}$ (GPa)	SD_{twin} (GPa)	SDM_{twin} (GPa)
20	5.92	0.60	0.06	6.02	0.192503	0.02
30	5.92	0.43	0.04	6.06	0.38399	0.04
40	5.94	0.41	0.04	6.25	0.305093	0.03
50	5.98	0.35	0.03	6.19	0.25	0.03

Table B.3: Radial dependence results for silver nanowires. This table displays the yielding stress of un-twinned, $\sigma_{untwinned}$, the standard deviation of the un-twinned, $SD_{untwinn}$, the standard deviation of the mean of the un-twinned, SDM_{untwin}, the yielding stress of twinned nanowires,$\sigma_{twinned}$, the standard deviation of the twinned nanowires,SD_{twin} , and the standard deviation of the mean for the twinned yielding stress, SDM_{twin}.

Radius (A)	$\sigma_{untwinned}$ (GPa)	SD (GPa)	SDM (GPa)	$\sigma_{twinned}$ (GPa)	SD (GPa)	SDM (GPa)
100	7.94	0.37	0.04	8.05	0.573263	0.06
300	5.79	0.46	0.05	6.18	0.550595	0.06
500	4.50	0.45	0.05	4.63	0.22686	0.02
800	2.53	0.32	0.03	2.78	0.19	0.02

Table B.4: Radial dependence results for silver nanowires. This table displays the difference in yielding stress, σ_{diff}, the error in calculating the difference using the standard deviation, $\delta\sigma_{diffSD}$, the error in calculating the difference using the standard deviation of the mean, , $\delta\sigma_{diffSDM}$, the normalized yielding stress,σ_{norm}, the error in calculating the normalized yielding stress using the standard deviation, $\delta\sigma_{normSD}$, and the error in calculating the normalized yielding stress using the standard deviation of the mean,$\delta\sigma_{normSDM}$.

Radius (A)	σ_{diff} (GPa)	$\delta\sigma_{diffSD}$ (GPa)	$\delta\sigma_{diffSDM}$ (GPa)	σ_{norm}	$\delta\sigma_{normSD}$	$\delta\sigma_{normSDM}$
100	0.11	0.95	0.09	0.01	0.12	0.01
300	0.40	1.01	0.10	0.07	0.18	0.02
500	0.12	0.68	0.07	0.03	0.15	0.02
800	0.24	0.51	0.05	0.10	0.21	0.02

Table B.5: Radial dependence results for copper nanowires. This table displays the yielding stress of un-twinned, $\sigma_{untwinned}$, the standard deviation of the un-twinned, $SD_{untwinn}$, the standard deviation of the mean of the un-twinned, SDM_{untwin}, the yielding stress of twinned nanowires,$\sigma_{twinned}$, the standard deviation of the twinned nanowires,SD_{twin} , and the standard deviation of the mean for the twinned yielding stress, SDM_{twin}.

Radius (A)	$\sigma_{untwinned}$ (GPa)	SD (GPa)	SDM (GPa)	$\sigma_{twinned}$ (GPa)	SD (GPa)	SDM (GPa)
20	9.11	0.74	0.07	9.43	0.46	0.05
25	9.29	1.24	0.12	9.44	0.44	0.04
30	9.20	0.56	0.18	9.41	0.69	0.07
35	9.06	0.52	0.05	9.31	0.99	0.10
40	9.19	0.18	0.02	9.41	0.59	0.06
45	9.09	0.85	0.08	9.38	0.45	0.05

Table B.6: Radial dependence results for copper nanowires. This table displays the difference in yielding stress, σ_{diff}, the error in calculating the difference using the standard deviation, $\delta\sigma_{diffSD}$, the error in calculating the difference using the standard deviation of the mean, , $\delta\sigma_{diffSDM}$, the normalized yielding stress,σ_{norm}, the error in calculating the normalized yielding stress using the standard deviation, $\delta\sigma_{normSD}$, and the error in calculating the normalized yielding stress using the standard deviation of the mean,$\delta\sigma_{normSDM}$.

Radius (A)	σ_{diff} (GPa)	$\delta\sigma_{diffSD}$ (GPa)	$\delta\sigma_{diffSDM}$ (GPa)	σ_{norm}	$\delta\sigma_{normSD}$	$\delta\sigma_{normSDM}$
20	0.32	1.20	0.12	0.03	0.13	0.01
25	0.15	1.68	0.17	0.02	0.18	0.02
30	0.21	1.25	0.25	0.02	0.14	0.03
35	0.25	1.51	0.15	0.03	0.17	0.02
40	0.22	0.77	0.08	0.02	0.08	0.01
45	0.29	1.30	0.13	0.03	0.15	0.01

Table B.7: Radial dependence results for copper nanowires. This table displays the yielding stress of un-twinned, $\sigma_{untwinned}$, the standard deviation of the un-twinned, $SD_{untwinn}$, the standard deviation of the mean of the un-twinned, SDM_{untwin}, the yielding stress of twinned nanowires,$\sigma_{twinned}$, the standard deviation of the twinned nanowires,SD_{twin} , and the standard deviation of the mean for the twinned yielding stress, SDM_{twin}.

Radius (A)	$\sigma_{untwinned}$ (GPa)	SD (GPa)	SDM (GPa)	$\sigma_{twinned}$ (GPa)	SD (GPa)	SDM (GPa)
100	12.46	0.04	0.00	12.25	1.14	0.11
300	9.24	0.53	0.05	9.32	0.79	0.08
500	7.01	1.03	0.10	7.24	0.39	0.04
800	4.35	0.76	0.08	4.92	0.33	0.03
1100	2.38	0.33	0.03	2.75	0.22	0.02

Table B.8: Radial dependence results for copper nanowires. This table displays the difference in yielding stress, σ_{diff}, the error in calculating the difference using the standard deviation, $\delta\sigma_{diffSD}$, the error in calculating the difference using the standard deviation of the mean, , $\delta\sigma_{diffSDM}$, the normalized yielding stress,σ_{norm}, the error in calculating the normalized yielding stress using the standard deviation, $\delta\sigma_{normSD}$, and the error in calculating the normalized yielding stress using the standard deviation of the mean,$\delta\sigma_{normSDM}$.

Radius (A)	σ_{diff} (GPa)	$\delta\sigma_{diffSD}$ (GPa)	$\delta\sigma_{diffSDM}$ (GPa)	σ_{norm}	$\delta\sigma_{normSD}$	$\delta\sigma_{normSDM}$
100	-0.21	1.17	0.12	-0.02	-0.09	-0.01
300	0.08	1.32	0.13	0.01	0.14	0.01
500	0.23	1.42	0.14	0.03	0.21	0.02
800	0.57	1.08	0.11	0.13	0.27	0.03
1100	0.37	0.54	0.05	0.15	0.25	0.02

Table B.9: Radial dependence results for nickel nanowires. This table displays the yielding stress of un-twinned, $\sigma_{untwinned}$, the standard deviation of the un-twinned, $SD_{untwinn}$, the standard deviation of the mean of the un-twinned, SDM_{untwin}, the yielding stress of twinned nanowires,$\sigma_{twinned}$, the standard deviation of the twinned nanowires,SD_{twin} , and the standard deviation of the mean for the twinned yielding stress, SDM_{twin}.

Radius (A)	$\sigma_{untwinned}$ (GPa)	SD (GPa)	SDM (GPa)	$\sigma_{twinned}$ (GPa)	SD (GPa)	SDM (GPa)
20	15.46	1.52	0.11	15.69	0.25	0.02
25	15.33	1.26	0.09	15.86	1.12	0.09
30	15.59	1.42	0.10	15.92	1.23	0.10
35	15.55	1.41	0.10	15.96	1.02	0.08
40	15.17	2.27	0.16	15.96	0.88	0.07
45	15.42	1.70	0.12	15.81	1.46	0.12

Table B.10: Radial dependence results for nickel nanowires. This table displays the difference in yielding stress, σ_{diff}, the error in calculating the difference using the standard deviation, $\delta\sigma_{diffSD}$, the error in calculating the difference using the standard deviation of the mean, , $\delta\sigma_{diffSDM}$, the normalized yielding stress,σ_{norm}, the error in calculating the normalized yielding stress using the standard deviation, $\delta\sigma_{normSD}$, and the error in calculating the normalized yielding stress using the standard deviation of the mean,$\delta\sigma_{normSDM}$.

Radius (A)	σ_{diff} (GPa)	$\delta\sigma_{diffSD}$ (GPa)	$\delta\sigma_{diffSDM}$ (GPa)	σ_{norm}	$\delta\sigma_{normSD}$	$\delta\sigma_{normSDM}$
20	0.23	1.77	0.13	0.01	0.12	0.01
25	0.53	2.38	0.18	0.03	0.16	0.01
30	0.33	2.65	0.20	0.02	0.17	0.01
35	0.40	2.43	0.18	0.03	0.16	0.01
40	0.79	3.16	0.23	0.05	0.22	0.02
45	0.39	3.16	0.24	0.03	0.21	0.02

Table B.11: Radial dependence results for nickel nanowires. This table displays the yielding stress of un-twinned, $\sigma_{untwinned}$, the standard deviation of the un-twinned, $SD_{untwinn}$, the standard deviation of the mean of the un-twinned, SDM_{untwin}, the yielding stress of twinned nanowires,$\sigma_{twinned}$, the standard deviation of the twinned nanowires,SD_{twin} , and the standard deviation of the mean for the twinned yielding stress, SDM_{twin}.

Radius (A)	$\sigma_{untwinned}$ (GPa)	SD (GPa)	SDM (GPa)	$\sigma_{twinned}$ (GPa)	SD (GPa)	SDM (GPa)
100	19.72	1.56	0.12	19.21	0.76	0.06
300	15.44	0.88	0.07	15.74	1.02	0.08
500	12.40	1.70	0.13	13.02	1.02	0.08
800	9.27	0.58	0.05	9.84	0.61	0.05
1100	6.32	0.48	0.04	7.15	0.48	0.04

Table B.12: Radial dependence results for nickel nanowires. This table displays the difference in yielding stress, σ_{diff}, the error in calculating the difference using the standard deviation, $\delta\sigma_{diffSD}$, the error in calculating the difference using the standard deviation of the mean, , $\delta\sigma_{diffSDM}$, the normalized yielding stress,σ_{norm}, the error in calculating the normalized yielding stress using the standard deviation, $\delta\sigma_{normSD}$, and the error in calculating the normalized yielding stress using the standard deviation of the mean,$\delta\sigma_{normSDM}$.

Radius (A)	σ_{diff} (GPa)	$\delta\sigma_{diffSD}$ (GPa)	$\delta\sigma_{diffSDM}$ (GPa)	σ_{norm}	$\delta\sigma_{normSD}$	$\delta\sigma_{normSDM}$
100	-0.51	2.33	0.18	-0.03	-0.12	-0.01
300	0.31	1.91	0.15	0.02	0.12	0.01
500	0.62	2.72	0.22	0.05	0.23	0.02
800	0.57	1.19	0.09	0.06	0.13	0.01
1100	0.83	0.96	0.08	0.13	0.16	0.01

Appendix C

Radial dependence extrapolated values

Table C.1: Extrapolated radial dependence for silver nanowires.

Ag	Radius (A)	Yielding Stress Twinned (GPa)	Yielding Stress Un-twinned (GPa)	Normalized Stress	Yielding Stress Difference (GPa)
	100	6.6	6.1	0.09	0.6
	150	6.9	6.2	0.1	0.9
	200	7.3	6.2	0.2	1.3
	250	7.6	6.3	0.2	1.6
	300	8.0	6.4	0.3	1.9

Table C.2: Extrapolated radial dependence for copper nanowires.

Cu	Radius (A)	Yielding Stress Twinned (GPa)	Yielding Stress Un-twinned (GPa)	Normalized Stress	Yielding Stress Difference (GPa)
	100	9.2	8.9	0.03	0.3
	150	9.1	8.8	0.04	0.3
	200	9.0	8.6	0.04	0.4
	250	8.8	8.4	0.04	0.4
	300	8.7	8.3	0.05	0.4

Table C.3: Extrapolated radial dependence for nickel nanowires.

Ni	Radius (A)	Yielding Stress Twinned (GPa)	Yielding Stress Un-twinned (GPa)	Normalized Stress	Yielding Stress Difference (GPa)
	100	16.2	15.1	0.07	1.1
	150	16.5	14.9	0.1	1.6
	200	16.7	14.7	0.1	2.0
	250	17.0	14.5	0.2	2.5
	300	17.3	14.3	0.2	3.0

Temperature dependence extrapolated values

Table C.4: Extrapolated temperature values for silver nanowires.

Ag	Temperature	Yielding Stress Twinned (GPa)	Yielding Stress Un-twinned (GPa)	Yielding Stress Normalized	Yielding Stress Difference (GPa)
	900K	1.9	1.6	0.1	0.2
	1000K	1.1	0.9	0.1	0.3
	1100K	0.4	0.1	0.1	0.3
	1200K	-0.4	-0.7	0.1	0.3

Table C.5: Extrapolated temperature values for copper nanowires.

Cu	Temperature	Yielding Stress Twinned (GPa)	Yielding Stress Un-twinned (GPa)	Yielding Stress Normalized	Yielding Stress Difference (GPa)
	1200K	1.4	0.8	0.2	0.6
	1300K	0.5	-0.2	0.2	0.7
	1400K	-0.4	-1.2	0.2	0.7

Table C.6: Extrapolated temperature values for nickel nanowires

Ni	Temperature	Yielding Stress Twinned (GPa)	Yielding Stress Un-twinned (GPa)	Yielding Stress Normalized	Yielding Stress Difference (GPa)
	1200K	5.4	4.3	0.1	1.1
	1300K	4.2	3.0	0.2	1.2
	1400K	3.0	1.7	0.2	1.3
	1500K	1.9	0.5	0.2	1.4
	1600K	0.7	-0.8	0.2	1.5

7.0 References

[1] Zhang, H., & Huang, H. (2009). Do twin boundaries always strengthen metal nanowires?. Nanoscale Research Letters, 34-38. doi: 10.1007/s11671-008-9198-1

[2] Nath, S., & Kim, S. (2012). On the elastic, elastic-plastic properties of au nanowires in the range of diameter 1-200nm. JOURNAL OF APPLIED PHYSICS, 112(12), doi: 10.1063/1.4770356

[3] Lucas, M., Leach, A., McDowell, M., Hunyadi, S., Gall, K., Murphy, C., & Riedo, E. (2008). Plastic deformation of pentagonal silver nanowires: Comparison between afm nanoindentation and atomistic simulations. PHYSICAL REVIEW B,77(24), doi: 10.1103/PhysRevB.77.245420

[4] Wu, B., Heidelberg, A., & Boland, J. (2005). Mechanical properties of ultrahigh-strength gold nanowires.Nature Materials, 4(7), 525-529. doi: 10.1038/nmat1403

[5] Jing, G., Duan, H., Sun, X., Zhang, Z., Xu, J., Li, Y., Wang, J., & Yu, D. (2006). Surface effects on elastic properties of silver nanowires: Contact atomic-force microscopy. PHYSICAL REVIEW B,73(23), doi: 10.1103/PhysRevB.73.235409

[6] Liang, H., Upmanyu, M., & Huang, H. (2005). Size-dependent elasticity of nanowires: Nonlinear effects. PHYSICAL REVIEW B, 71(24), doi: 10.1103/PhysRevB.71.241403

[7] Zhu, Y., Qin, Q., Xu, F., Fan, F., Ding, Y., Zhang, T., Wiley, B., & Wang, Z. (2012). Size effects on elasticity, yielding, and fracture of silver nanowires: In situ experiments. PHYSICAL REVIEW B, 85(4), doi: 10.1103/PhysRevB.85.045443

[8] Deng, C., & Sansoz, F. (2009). Size-dependent yield stress in twinned gold nanowires mediated by site-specific surface dislocation emission.APPLIED PHYSICS LETTERS, 95(9), doi: 10.1063/1.3222936

[9] Afanasyev, K., & Sansoz, F. (2007). Strengthening in gold nanopillars with nanoscale twins. NANO LETTERS, 71(7), 2056-2062. doi: 10.1021/nl070959l

[10] Deng, C., & Sansoz, F. (2009). Fundamental differences in the plasticity of periodically twinned nanowires in au, ag, al, cu, pb and ni. ACTA MATERIALIA, 57(20), 6090-6101. doi: 10.1016/j.actamat.2009.08.035

[11] Wu, H., Soh, A., Wang, X., & Sun, Z. (2004). Strength and fracture of single crystal metal nanowire. KEY ENGINEERING MATERIALS, 261-263, 33-38.

[12] Wang, W., Yi, C., & Fan, K. (2013). Molecular dynamics study on temperature and strain rate dependences of mechanical tensile properties of ultrathin nickel nanowires. TRANSACTIONS OF NONFERROUS METALS SOCIETY OF CHINA, 23(11), 3353-3361. doi: 10.1016/S1003-6326(13)62875-7

[13] Wang, W., Yi, C., & Fan, K. (2013). Molecular dynamics study on temperature and strain rate dependences of mechanical tensile properties of ultrathin nickel nanowires. *TRANSACTIONS OF NONFERROUS METALS SOCIETY OF CHINA*, *23*(11), 3353-3361. doi: 10.1016/S1003-6326(13)62875-7

[14] Wu, Z., Zhang, Y., Jhon, M., Greer, J., & Srolovitz, D. (2013). Nanostructure and surface effects on yield in cu nanowires. ACTA MATERIALIA, 61(6), 1831-1842. doi: 10.1016/j.actamat.2012.11.053

[15] Cao, A., Wei, Y., & Mao, S. (2007). Deformation mechanisms of face-centered-cubic metal nanowires with twin boundaries. APPLIED PHYSICS LETTERS, 90(15), doi: 10.1063/1.2721367

[16] Pastor-Abia, L., Caturla, M., SanFabian, E., Chiappe, G., & Louis, E. (2008). Stress-strain curves of aluminum nanowires: Fluctuations in the plastic regime and absence of hardening. PHYSICAL REVIEW B, 78(15), doi: 10.1103/PhysRevB.78.153410

[17] Mirabbaszadeh, K., Nayebi, P., & Zaminpayma, E. (2010). Molecular dynamics simulation of mechanical properties of ni-al nanowires.COMPUTATIONAL MATERIALS SCIENCE,50(1), 10-14. doi: 10.1016/j.commatsci.2010.06.03

[18] Ma, F., Song, Z., Li, Y., & Xu, K. (2010). Plastic deformation in bi-metal multilayer nanowires.MICROELECTRONIC ENGINEERING, 87(3), 426-429. doi: 10.1016/j.mee.2009.06.010

[19] Sun, M., Cao, R., Xiao, F., & Deng, C. (2013). Five-fold twin and surface groove-induced abnormal size- and temperature-dependent yielding in ag nanowires. SCRIPTA MATERIALIA, 69(3), 227-230. doi: 10.1016/j.scriptamat.2013.04.002

[20] Muller-Plathe, F. (1997). *Problem solving in computational molecular science*. (Vol. 500, pp. 389-412). Dordrecht: Kluwer Academic Publishers.

[21] Haile, J. M. (1992). *Molecular dynamics simulation*. (pp. 1-141). New York: John Wiley & Sons

[22] Leach, A. (2001). *Molecular modeling principles and applicationis*. (2nd ed., pp. 353-409). London: Pearson Education Limited.

[23] Foiles, S. M., Baskes, M. I., & Daw, M. S. (1986). Embedded-atom-method functions for the fcc metals cu, ag, au, ni, pd, pt, and their alloys. *Physical Review B*, *33*(12), 1986.

[24] Mishin, Y., Farkas, D., Mehl, M. J., & Papaconstantopoulos, D. A. (1999). Interatomic potentials for monoatomic metals from experimental data and ab initio calculations. *Physical Review B*,*59*(5), 3393-3407.

[25] Williams, P. L., Mishin, Y., & Hamilton, J. C. (2006). An embedded-atom potential for the cu-ag system.*Modelling and Simulation in Materials Science and Engineering*, *14*, 817-833. doi: 10.1088/0965-0393/14/5/002

[26] S. Plimpton, Fast Parallel Algorithms for Short-Range Molecular Dynamics, J Comp Phys, 117, 1-19 (1995)

[27] Taylor, J. (1997). *Error analysis*. (2nd ed., pp. 1-110). United States of America: University Science Books.

[28] W. M. Haynes, ed., CRC Handbook of Chemistry and Physics, 94th Edition (Internet Version 2014), CRC Press/Taylor and Francis, Boca Raton, FL

[29] Hosford, W. (2008). *Materials for engineers*. (pp. 28-60). New York, NY: Cambridge University Press